Cartilage biomechanics: From the basic facts to the challenges of tissue engineering

Noémie Petitjean, Patrick Cañadas, Pascale Royer, Danièle Noël, Simon Le Floc'h

Received: 11 July 2022 | Revised: 7 November 2022 | Accepted: 22 November 2022

DOI: 10.1002/jbm.a.37478

REVIEW ARTICLE

Society For Biomaterials | WILEY

Cartilage biomechanics: From the basic facts to the challenges of tissue engineering

Noémie Petitjean[1] | Patrick Canadas[2] | Pascale Royer[2] | Danièle Noël[1,3] | Simon Le Floc'h[2]

[1]IRMB, University of Montpellier, INSERM, Montpellier, France

[2]LMGC, University of Montpellier, CNRS, Montpellier, France

[3]Clinical Immunology and Osteoarticular Disease Therapeutic Unit, Department of Rheumatology, CHU Montpellier, France

Correspondence
Simon Le Floc'h, LMGC - UMR 5508 Université de Montpellier, CC048 163 rue Auguste Broussonnet 34090 Montpellier, France.
Email: simon.le-floc-h@umontpellier.fr

Funding information
CNRS (AAP "Osez l'interdesciplinarité 2018"), Grant/Award Number: MoTiV Project; French State grant managed by the French National Research Agency under the Investments for the Future programme, Grant/Award Number: ANR-10-LABX-20

Abstract

Articular cartilage (AC) is the thin tissue that covers the long bone ends in the joints and that ensures the transmission of forces between adjacent bones while allowing nearly frictionless movements between them. AC repair is a technologic and scientific challenge that has been addressed with numerous approaches. A major deadlock is the capacity to take in account its complex mechanical properties in repair strategies. In this review, we first describe the major mechanical behaviors of AC for the non-specialists. Then, we show how researchers have progressively identified specific mechanical parameters using mathematical models. There are still gaps in our understanding of some of the observations concerning AC biomechanical properties, particularly the differences in extracellular matrix stiffness measured at the microscale and at the millimetric scale. Nevertheless, for bioengineering applications, AC repair strategies must take into account what are commonly considered the main mechanical features of cartilage: its ability to withstand high stresses through three main behaviors (elasticity, poroelasticity and swelling). Finally, we emphasize that future studies need to investigate AC mechanical properties at different scales, particularly the gradient of mechanical properties around cells and across the cartilage depth, and the differences in mechanical properties at different scales. This multi-scale approach could greatly enhance the success of AC restorative approaches.

KEYWORDS
articular cartilage, biomechanics, mechanical properties, multi-scale, tissue engineering, Young's modulus

1 | INTRODUCTION

Articular cartilage (AC) is the thin tissue that covers the long bone ends in the joints and that ensures the transmission of forces between adjacent bones, while allowing nearly frictionless movements between them.[1] Trauma- and disease-related AC injuries represent an increasing public health problem, particularly due to population aging. Osteoarthritis (OA) is the most prevalent rheumatic disease, and is associated with several risk factors, including age, obesity and biomechanical dysfunction.[2–9] OA is characterized by cartilage degradation and modifications in its composition that affect its mechanical properties. Therefore, understanding the biomechanical changes in OA cartilage is interesting to identify the structural features and molecular signaling that characterize healthy cartilage.

Danièle Noël and Simon Le Floc'h contributed equally to this work.

AC has limited healing and repair capacities.[10] Besides pain management, several surgical techniques are used in the clinics, including microfracture, mosaicplasty, and autologous chondrocytes implantation.[11] Some tissue engineering techniques based on different scaffold types also have been tested in the clinics.[12–16] However, their benefits are frequently not long-lasting and the biomechanical properties of the repaired cartilage, often associated with a fibrocartilage phenotype, are generally different than those of the original cartilage.[11,17] A major clinical and technological challenge in tissue engineering is the capacity to mimic AC biomechanical properties in a sustainable manner, without deformation of the substitute material over time. Indeed, AC is continuously subjected to stress, but in physiological conditions, it can deform without injury. Although it is difficult to measure AC deformation directly in vivo, some data have been obtained using imaging techniques or instrumented implants with pressure or force sensors, particularly in hip and knee joints.[18–22] Mechanical stress in human joints has been precisely measured, and the results have been extrapolated to evaluate the physiological loads to the AC. For several types of physical activities, the obtained experimental data are provided in terms of contact area, pressure and/or force, expressed as body weight percentage (%BW). For example, for daily-life movements, the contact force acting on the hip joint and the tibial plateau measured with implantable sensors ranges between 107% BW and 346% BW.[18,20,21] Furthermore, it is important to note that this contact force is not evenly distributed over the cartilage surface. Indeed, the sensor surface is subject to a pressure that varies locally between −0.13 MPa (the minus sign indicates an attractive or cohesive force) to +7.14 MPa (the positive value reveals a compressive force) during standing.[20] Few studies evaluated AC deformation, and most of them used magnetic resonance imaging (MRI). Depending on the joint (tibiofemoral, ankle joint) or stress type (joint flexion, walking, weight-bearing single-leg lunge), the peak deformation in the contact zone varies between −7% and −30% of the initial thickness.[19,22–25]

Better understanding AC mechanical behaviors and the quantification of the related parameters are crucial issues for developing efficient AC repair approaches that can withstand in vivo loads. This engineered tissue must display sufficient strength and moderate stiffness to resist mechanical loads and absorb part of the contact energy between the related bones. On the other hand, the extracellular matrix (ECM) around cells in the cartilage tissue must behave like a very soft tissue to maintain the right biomechanical cell environment. Many studies have evaluated AC biomechanical properties using different (i) tissue samples, (ii) mechanical models, (iii) experimental techniques, and (iv) tests, thus leading to an important variability of the resulting volumetric mechanical properties (i.e., the properties of the overall volume of the tested sample). Most studies have focused on the apparent Young's modulus that can be measured with a compression test and is widely used to evaluate AC quality. However, because of the complexity of AC composition and structure at different scales, this parameter does not give sufficient information. Other volumetric mechanical properties, particularly those linked to time-dependent and multi-scale behaviors have been little explored. The mechanical properties of AC surface (i.e., AC tribology, the study of contact mechanics of AC) have been studied for several decades (for review, see References [26,27]). This research field requires specific theoretical and experimental tools and is out of the scope of the present article.

The objective of this review is to give an update of what is known about AC mechanical behaviors, and to highlight specific behaviors and properties that have been observed in native AC but are still difficult to mimic in the current bioengineering approaches. This review will focus on (1) the basic knowledge of AC mechanical behavior in relation to its biochemical and structural composition at different scales, (2) the parameters commonly used to estimate the mechanical properties of healthy and OA AC, and (3) the tissue engineering challenges to mimic AC mechanical properties.

2 | BASIC KNOWLEDGE ON AC MECHANICAL BEHAVIOR IN RELATION WITH ITS BIOCHEMICAL COMPOSITION

2.1 | AC composition and structure

AC is a conjunctive tissue composed mainly of ECM (98% of the volume) and chondrocytes (2% of the volume), a terminally differentiated cell type.[1] Chondrocytes are highly specialized cells that synthesize and degrade the ECM. The ECM is mainly composed of water that represents 70%–80% of its weight. In AC, proteoglycans and type II collagens (COL II) are the main ECM components, followed by type VI, IX and XI collagens. Proteoglycans and collagens account for 5%–15% and 60%–70% of the dry weight of ECM, respectively. COL II fibrils are bundles of fibers fixed by type IX and XI collagens,[28,29] whereas type VI collagens are small sparse fibers that surround chondrocytes. Aggrecan, which represents 90% of AC proteoglycans is composed of lateral chains of sulfated glycosaminoglycans (GAG), namely chondroitin sulfates and keratan sulfates.[30] Aggrecan is directly linked to hyaluronic acid (HA) or via the link protein and fills the space between collagen fibrils. The carboxyl and sulfate groups of carbohydrate chains bind cations and about 30% of the water in AC.[31,32] Biglycan, decorin and fibromodulin are small PGs present in the ECM that play a role in fibrillogenesis by interacting with COL II fibers.[33–35] Biglycan and decorin, which are also found close to chondrocytes, participate in their anchoring in ECM by interacting directly with COL VI, and COL II fibers via matrilines 1 and 3.[36] Perlecan is directly in contact with chondrocytes or via integrins and is associated with Col VI in the pericellular matrix.[37–40] Several other molecules (e.g., anchorin CII, CD44, integrins, fibronectin, link, cartilage oligomeric matrix protein) allow connecting chondrocytes to ECM.[35,36,40–42]

AC is a heterogeneous tissue with a specific organization in three zones[1] (Figure 1A). In the superficial zone, chondrocytes are flattened and parallel to the articular surface. COL II fibrils are thin (diameter of 20 nm), parallel to the articular surface and are mainly oriented in the direction of articular rotation (split line). In the middle transitional zone, chondrocytes are spherical and at low density. COL II fibrils are thicker, separated in two sub-groups: primary fibrils that cross the

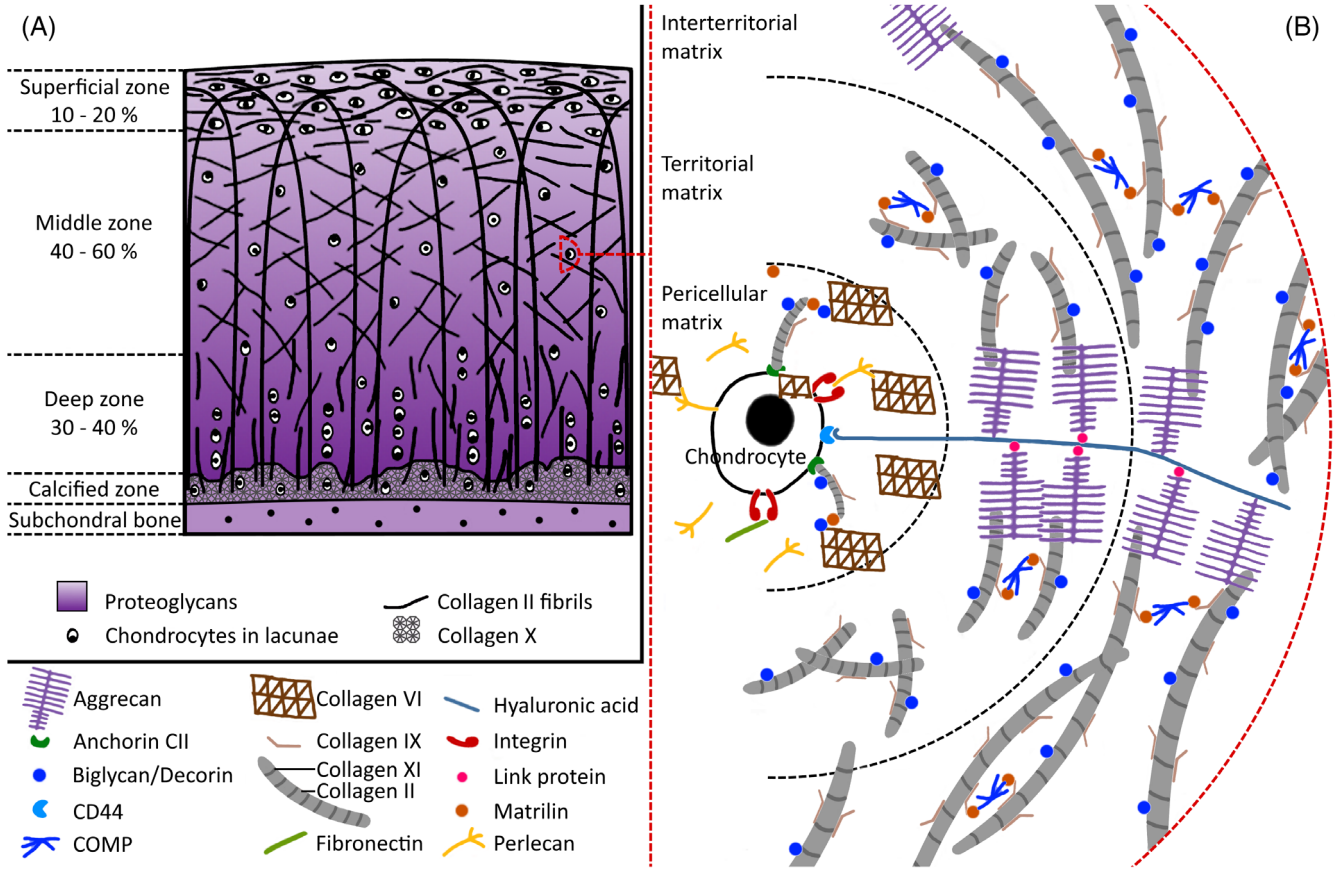

FIGURE 1 Structural organization of articular cartilage. (A) Zonal distribution from the surface to the subchondral bone. In the three first zones, proteoglycan concentration increases with the depth (darker purple). Primary collagen II fibrils have an arcade-like structure (biggest fibrils), whereas secondary collagen II fibrils are parallel to the articular surface in the superficial zone and more randomly oriented in other zones (smaller fibrils). Chondrocytes are more numerous in the superficial zone and are organized in columns in the deep zone. The calcified zone is composed of sodium hyaluronate, nanohydroxyapatite and type X collagen produced by few hypertrophic chondrocytes. (B) Regional distribution of the extracellular matrix around a chondrocyte. Chondrocytes are linked to the extracellular matrix by many molecules found in the pericellular matrix (anchorin CII, CD44, Integrins, fibronectin, perlecan, matrilin, biglycan, and decorin). In the territorial matrix, the size of collagen II fibrils, mediated by collagen IX and collagen XI fibers and proteoglycans like biglycan and decorin, and the number of connections between collagen fibrils and proteoglycans by cartilage oligomeric matrix proteins (COMP) and matrilins, increase until the interterritorial zone. Aggrecans are linked to hyaluronic acids, directly or via link proteins, and to collagen II fibrils

tissue and have an arcade-like structure, and secondary thinner fibrils that are obliquely and randomly oriented.[43–45] It can be noted that few type X collagen fibers are present in colocalization with the collagen fibril arcades.[46] In the deep zone, chondrocytes are organized in columns and elongated perpendicularly to the articular surface. COL II fibrils are thicker (diameter of 70–120 nm) but fewer in number, and oriented perpendicularly to the articular surface. All zones contain proteoglycans with a diameter of only few nanometers, and their concentration increases with depth.[47] A fourth deeper zone, called calcified zone, is composed of sodium hyaluronate, nanohydroxyapatite and type X collagen produced by few hypertrophic chondrocytes. Type X collagen fibers are organized in hexagonal lattice-like structure.[48,49]

AC can also be divided in three radial regions from the chondrocytes (Figure 1B). The pericellular matrix is the first region that surrounds the chondrocytes. Its thickness is between 2 and 5 µm and increases from the AC surface to the deepest zone.[50] The pericellular matrix contains many proteins and type VI collagen fibers that are mainly oriented in the direction of COL II fibrils.[51] Then, the territorial matrix forms an irregular fibrillar coat around one or more chondrocytes.[44] It contains thin COL II fibrils, and is richer in proteoglycans.[52] The interterritorial matrix is the largest region and contains highly organized and large COL II fibrils and many proteoglycans. As shown in Figure 1B, many proteins create links between chondrocytes, COL II fibrils and proteoglycans through the different regions.

AC is a highly organized conjunctive tissue at three important scales: the fibril scale (nanometric), the cell scale, and the tissue scale.[53] The heterogeneous distribution of its components, the specific fibril orientation in the different zones, the presence of free water in the dense structure of the ECM, and the organization around chondrocytes create complex mechanical behaviors. Different AC biomechanical behaviors are associated with AC vertical (from the surface to the subchondral bone) and radial structures (around the chondrocyte) that can be referred as behaviors at the millimeter scale

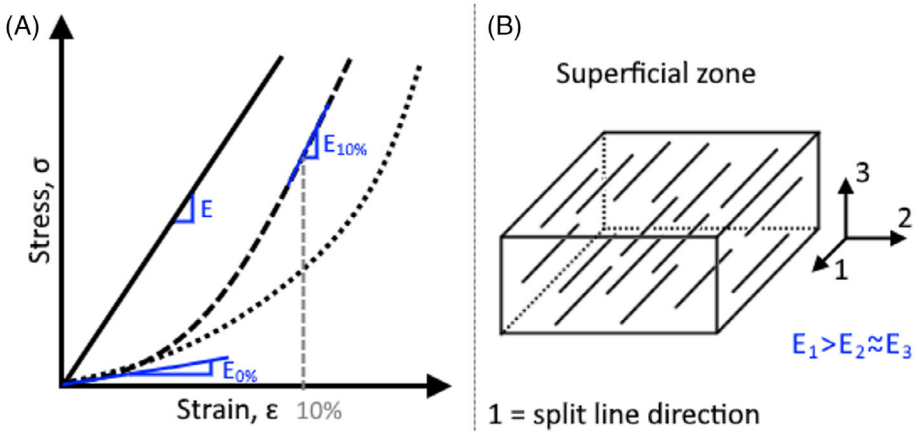

FIGURE 2 The elastic properties of a material are characterized through its stress–strain curve (A) and are different according to the directions of space (B). (A) Stress–strain curves describe both the linear (plain curve) and non-linear (dotted curve) elastic behavior of materials. Articular cartilage displays a linear elastic behavior with a non-linear toe-region (dashed curve). The Young's modulus (E) of the material is given by the stress to strain ratio. It can be determined for different strain levels ($E_{0\%}$ and $E_{10\%}$). (B) In the superficial zone of articular cartilage, collagen II fibrils are preferentially oriented in the split line direction, and this causes anisotropy by increasing the Young's modulus measured in tension in the split line direction (E_1) compared with the other two directions (E_2 and E_3)

and microscale, respectively. The biomechanical properties of AC are dependent of its ultrastructural organization, which is associated to the biochemical composition and cell–cell and ECM-cell interactions.[54] Any small alteration in these properties will drastically alter tissue biomechanics.[55] This is notably the case in pathological situations such as OA where over-expression of type X collagen, metalloproteinases and degradation of MEC components will affect the structure of the tissue.[56]

2.2 | Mechanical behaviors

AC is a mechanosensitive tissue that can absorb and distribute physiological loads for many years without failure. To do so, AC exhibits specific mechanical behaviors to withstand the weight of external loads. Importantly, AC mechanical properties vary in function of the location (heterogeneity), direction (anisotropy), and scale (multi-scale). As it is difficult to perform in vivo measurements, most mechanical tests to evaluate AC mechanical behavior are carried out in vitro using AC biopsies. To easily understand AC biomechanics, we divided AC behaviors in two categories that allow highlighting specific mechanical features: time-independent and time-dependent behaviors.

2.2.1 | Time-independent behaviors

Elastic behavior describes the ability to follow a unique relationship between applied force and tissue deformation, regardless of how the tissue is mechanically loaded. Thus, if elastic, a tissue withstands reversible deformation by returning to its initial shape after the mechanical load is removed. AC if not damaged, returns to its initial state after load removal (spring back). AC reversible deformation is explained by the nature of the interconnections of COL II and proteoglycans, and water that flows out and in the tissue during deformation and spring back. However, the relationship between the applied force on an AC sample and its deformation during the loading phase is not the same as during the unloading phase, which is common for soft tissues.[57] Thus, AC cannot be considered to have elastic behavior. Nevertheless, the concept of pseudo-elasticity proposed by Fung allows the identification of distinct apparent pseudo-elastic behaviors depending on the loading conditions. Most of the studies estimating the elastic behavior of AC use the concept of pseudo-elasticity in an implicit manner: rather than pure elastic parameters, they report apparent ones. Pseudo-elasticity has been the first AC behavior assessed using compression, shear, traction, and indentation tests. Of importance, for a given stress (e.g., a load), the strain differs depending on the sample rigidity (i.e., stiffness): the higher the apparent stiffness of AC, the lower its deformation (Figure 2A).[58]

AC compressible behavior contributes to its pseudo-elastic behavior and is due to volume changes during loading. AC includes a solid phase (the ECM) and a fluid phase that are both considered incompressible because their respective volume is assumed not to change during the overall deformation. AC volume change during compression is caused by the loss of fluid. Therefore, in most situations, to explain its elastic behavior, AC must be assimilated to a compressible tissue to take in account the loss of fluid.

AC is naturally pre-stressed without any mechanical action (including gravity and muscle forces) because of the osmotic pressure in the tissue. Indeed, a mechanical equilibrium is maintained by the major ECM components.[59] Briefly, the negative charges of proteoglycans retain cations, making the tissue hypertonic, and water enters the tissue and creates an osmotic pressure. Moreover, repulsive forces caused by these negative charges tend to separate molecules, leading to tissue swelling. In response to this swelling behavior,

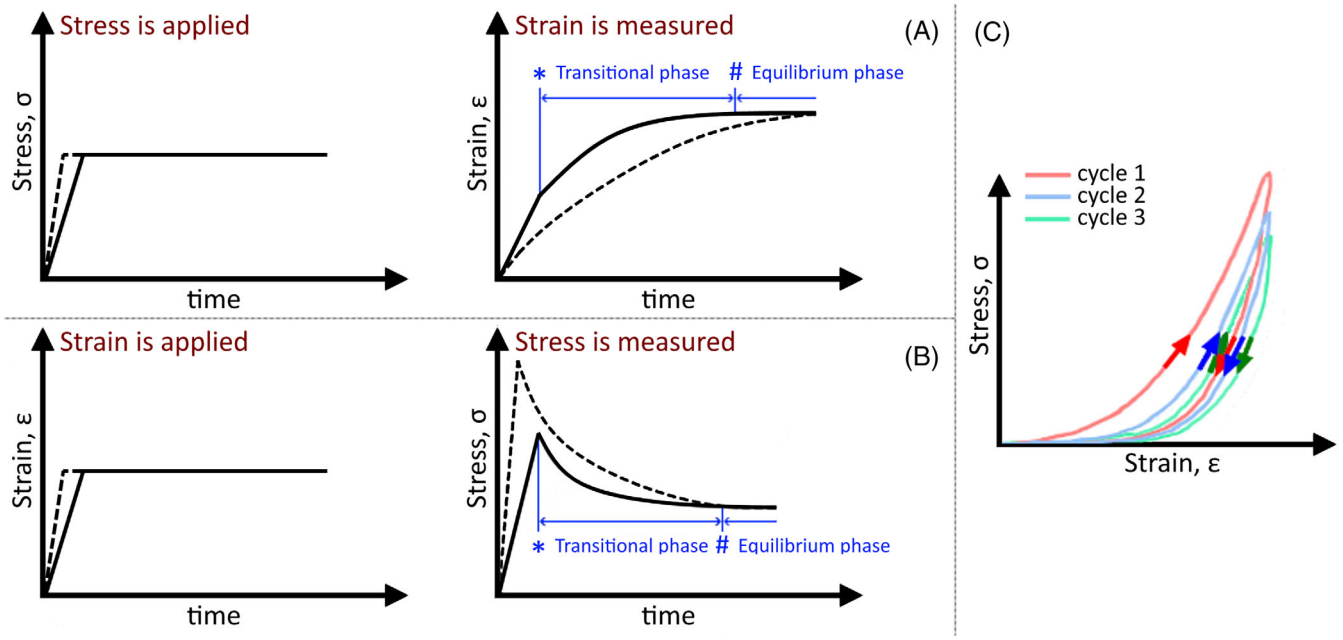

FIGURE 3 Stress–strain curves describe the damping behavior of articular cartilage. (A) During a creep test, the stress level is reached with a loading rate (i.e., a loading speed) and then maintained. An instantaneous strain level (*) is obtained during loading and then it creeps during the transition phase until it reaches the equilibrium state (#). Higher loading rate (dashed lines) result in lower instantaneous strain levels and longer transition phases to reach the equilibrium. (B) During a relaxation test, the strain level is reached with a loading rate and then is maintained. The instantaneous stress level (*) is obtained during loading, and then it relaxes during the transition phase until it reaches the equilibrium state (#). Higher loading rates (dashed lines) result in higher instantaneous stress levels and longer transition phases to reach the equilibrium. (C) During dynamic loading of the articular cartilage, several load and release cycles are performed. This leads to loops of stress–strain curves. The area in these loops represents the energy dissipated and/or stored by the sample during the loading. Several cycles are required to reach the load-release equilibrium

COL II fibrils and their cross-linked copolymers are stretched, and due to their stiffness, they limit the tissue expansion. This balance between repulsive and tensile forces enhances the stiffness of AC that is thus pre-stressed. Finally, this force balance changes when an external load is applied, leading to a new mechanical equilibrium.

2.2.2 | Time-dependent behaviors

AC displays a reversible elastic behavior between two equilibrium states of deformation. A time, called transitional phase, is necessary to reach each equilibrium state. During the transitional phase, strain or stress values change, indicating that AC behaviors are time dependent.

AC creep and relaxation behaviors are traditionally called viscous behavior. The creep behavior (Figure 3A) corresponds to the strain changes during the application of a constant stress. This behavior corresponds to the slow adaptation of the shape of the sample submitted to a constant force. The relaxation behavior (Figure 3B) corresponds to the stress changes during the application of a constant strain. This behavior corresponds to the slow adaptation of the reaction force at the contact point, while the imposed displacement remains constant. Two origins of viscous behaviors have been described in the literature.[60] The flow-dependent viscous behavior or poroelastic behavior is due to AC porous structure and involves the flow of a viscous fluid out of the solid phase pores. This flow is not instantaneous, thus inducing resistive forces that increase the tissue total reaction force. The flow-independent viscous behavior or viscoelastic behavior comes from the ECM viscosity due to the presence of COL II fibrils and proteoglycans that slide relative to each other and create frictions,[61] thus increasing the tissue reaction force. Therefore, during the transitional phase of creep or relaxation, part of the energy required to deform the tissue is lost through the viscous behaviors of the solid and fluid phases, and the sample deformation increases (creep) or the force it delivers decreases (relaxation) (Figure 3A,B).

AC hysteretic behavior is characterized by the difference between the load and unload phases of the stress–strain curve that describes a loop (Figure 3C). This characterizes an energy loss or storage during the load and release cycle. It is used to well characterize the capacity of AC to dissipate mechanical energy and/or to store mechanical energy. Basically, AC can be considered as a mechanical energy transmitter which consumes (i.e., either dissipates or stores) a non-negligible part of the mechanical energy that it transmits from one bone to another. Hysteresis is partly the result of AC time-dependent behaviors and might also be associated with microstructural or molecular rearrangements. The transient phase of hysteresis loops during which their shape and amplitude change can be observed also during the repetition of loading cycles until they

reach an equilibrium (i.e., their shape and amplitude do not change any longer). During the transitional phase, stress and the area in the center of the hysteresis loop decrease. In other words, the energy loss and the tissue stiffness decrease until an equilibrium is reached.[62] This may be due to a reorganization of COL II fibrils until they reach an optimal position in response to the stimulus, revealing micro-structural rearrangements.

Time-dependent behaviors are also velocity-dependent (i.e., loading rate-dependent). Typically, as the loading rate increases, AC apparent stiffness increases (Figure 3A,B).[63] These changes are related to the fluid capacity to flow out and to the solid phase viscosity. This leads to different apparent behaviors of AC depending on the loading rate.[64,65] At very small loading rate values (<<10^{-4} strain/s), the velocity allows the optimal solid matrix reorganization without energy dissipation. Thus, the temporal behaviors of the fluid and solid phases are negligible and cannot be measured as a supplementary reaction force. In this case, the behavior of a compressible solid phase without the fluid phase, therefore time-independent, could be considered as representative. Conversely, at very high loading rates (>1 strain/s), there is not enough time to drain the fluid out of the solid phase and to reorganize the COL II fibrils optimally,[64] thus leading to a time-independent behavior and the absence of hysteresis.[66] In this case, AC has an apparent incompressible solid behavior. Finally, at loading rates closer to the physiological range, the tissue exhibits a poroviscoelastic and a hysteretic behavior. The stress of the dynamic response increases in a non-linear manner with the loading rate (Figure 3B).[63,64] Moreover, the area of the hysteresis loop decreases with the loading rate, showing that energy dissipation is frequency-dependent.[66]

In general, the equilibrium elastic modulus is determined using very low loading rates (<<10^{-4} strain/s), whereas the dynamic elastic modulus is calculated at higher loading rates. Importantly, this loading rate-dependency implies that the mechanical properties of AC samples, calculated using the same technique and test, could be compared only if they concern equilibrium or dynamic data obtained at a similar loading rate.

2.2.3 | Non-linear, heterogeneous, and anisotropic behaviors

AC non-linear behavior is related to changes of mechanical behaviors observed with increasing loading amplitudes and rates. Stress (or strain) hardening defines an increase in AC stiffness with the increasing load.[67,68] This means that for the same strain increment, the stress increment will be greater at high strain values than at low strain values (Figure 2A, dotted curve). A gradual recruitment of COL II fibrils, which also have a non-linear behavior, and changes in their orientation increase the tension rigidity.[69,70] Moreover, the structural or geometrical non-linearity is due to the crosslinked polymer recruitment during stretching. In some cases, after the total recruitment of the fiber network, the stiffness does not change, thus exhibiting a linear behavior at high strain level. In this case, the stress–strain curve displays a toe-region with a non-linear behavior followed by a linear behavior with increasing strain (Figure 2A, dashed curve).[71] Finally, ECM reorganization during compression changes the fluid phase flow leading to a non-linear change of time-dependent behaviors.[5,72]

The anisotropic behavior of native AC is related to the different orientation of type II and type VI collagen fibers in the three zones. This implies that the mechanical properties should be direction dependent. For example, in the superficial zone, COL II fibrils are organized parallel to the AC surface and make the tissue stiffer in the split line direction (Figure 2B).

AC heterogeneous behavior is related to variations of its mechanical properties in function of the composition and of the COL II fibril and proteoglycan gradients in the different regions (Figure 1A).

To summarize, AC complex composition and structure lead to time-independent and time-dependent behaviors. These behaviors have been experimentally observed and vary in the tissue according to its depth and distance from chondrocytes, to the direction of the main deformation, and to the deformation state. Specific techniques are used, mainly indentation techniques (see Section 4), to capture these behaviors at the nano, micro and tissue scales. In the next section, we describe some AC differences at different scales and locations within the tissue using specific parameters.

3 | MECHANICAL PROPERTIES

3.1 | How AC mechanical behaviors are modeled

The different AC behaviors described in the previous section can be studied and quantified using an experimental technique to drive the mechanical test and a mathematical model. Indeed, besides data-driven computational mechanic approaches based on a huge number of experiments,[73,74] modeling of deformable bodies is widely used to predict the mechanical response of a sample submitted to a specific load. The simplest model is a spring in which the force is proportional to the distance from its equilibrium length. In this case, the model is represented by the equation that links the force to the displacement. In a more general way, modeling predicts physical parameters from other physical parameters. A model uses assumptions that lead to an incomplete description of the experimental observations. In the spring model, the parameter that quantifies the proportionality between the two physical quantities (the spring constant) is the model parameter that fully defines the relationship between force and displacement. If the force increases non-linearly with the displacement (no proportionality), the linear spring model is not suitable to describe this behavior. Thus, AC complex behaviors cannot be described by a simple model. Simple models, with relevant assumptions, can still be used, but caution is needed. Several experimental techniques have been developed to drive load and measure the sample response, and they can be chosen in function of the mechanical properties to be investigated (Table 1).

AC mechanical properties have been widely investigated (i) to obtain basic knowledge and to understand cartilage biomechanics, (ii) to describe the consequences of cartilage development and

TABLE 1 Non-exhaustive list of techniques used to mechanically characterize articular cartilage

	Technique	Scheme of the technique		Stress	Strain	Elastic parameter	Poisson ratio
		Before	After				
A	Unconfined compression	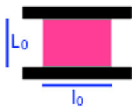		$\sigma_y = \frac{F}{S}$	$\varepsilon_y = \frac{\Delta L}{L_0}$ $\varepsilon_x = \frac{\Delta l}{l_0}$	Young's modulus $E = \frac{\sigma_y}{\varepsilon_y}$	$\nu = \frac{-\varepsilon_x}{\varepsilon_y}$
B	Traction			$\sigma_y = \frac{F}{S}$	$\varepsilon_y = \frac{\Delta L}{L_0}$ $\varepsilon_x = \frac{\Delta l}{l_0}$	Young's modulus $E = \frac{\sigma_y}{\varepsilon_y}$	$\nu = \frac{-\varepsilon_x}{\varepsilon_y}$
C	Confined compression	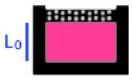	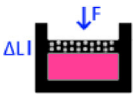	$\sigma_y = \frac{F}{S}$	$\varepsilon_y = \frac{\Delta L}{L_0}$	Aggregate modulus Ha $= \frac{\sigma_y}{\varepsilon_y}$	$\nu = 0$
D	Indentation	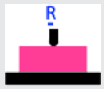	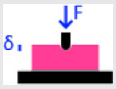			Young's modulus $E = \frac{3F(1-\nu^2)}{4R^{1/2}\delta^{3/2}}$	
E	Shear	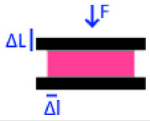	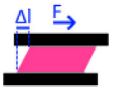	$\sigma_{xy} = \frac{F}{S}$	$\varepsilon_{xy} = \frac{\Delta l}{L_0}$	Shear modulus $G = \frac{\sigma_{xy}}{\varepsilon_{xy}}$	
F	Micro/nano indentation					Young's modulus $E = \frac{3F(1-\nu^2)}{4R^{1/2}\delta^{3/2}}$	
G	Micropipette aspiration		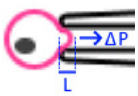	$\sigma = \Delta P$		Young's modulus $E = \frac{3a\Delta P\varphi(\eta)}{2\pi L}$, $\eta = \frac{b-a}{a}$ $\phi(\eta)$ from the punch model of Theret et al. (1988)[75]	

Note: At the millimetric scale, the articular cartilage mechanical properties can be determined by applying a force (F) that leads to a stress (σ), when knowing the sample surface (S) and strains (ε) during different mechanical tests. The Young's modulus (E) and Poisson's ratio (ν) can be calculated using unconfined compression (A) and tension (B) tests. The aggregate modulus (Ha) is determined using confined compression (C). An indentation test (D) can be used to determine a local Young's modulus. The equation indicated for the evaluation of E with the indentation test is valid for spherical tips with a radius R and an indentation depth δ. The shear modulus (G) is calculated using shear tests (E). At the microscale, the Young's modulus of the extracellular matrix can be calculated using micro or nanoindentation tests (F) and an equation adapted for spherical tips. Micropipette aspiration (G) is a technique used to determine the Young's modulus of chondrocytes and chondrons with the punch model, when knowing the difference in the applied pressure, the micropipette inner (A) and outer (B) radius, and the length of the sample that enters the micropipette (L).

pathologies, (iii) to investigate how to mimic this tissue, especially in the field of cartilage engineering.

3.2 | Pseudo-elastic properties

3.2.1 | Parameters required for the characterization of AC pseudo-elastic behavior

Generally, cylindrical AC biopsies are used for measuring compression and shear stress responsive forces. In most studies, AC is considered a purely elastic material (neither poroelastic nor viscoelastic). The transient (time-dependent) responses of AC samples to mechanical loads is not considered. This assumption helps to simplify the models and experimental setups used to estimate AC elastic properties. In solid mechanics, the elasticity of a material can be described by two parameters: the elastic modulus and the Poisson's ratio that quantify the material stiffness and compressibility, respectively. Different elastic moduli, not interchangeable, can be defined depending on the technique used and thus the test configuration: Young's modulus, aggregation modulus or shear modulus.

The Young's modulus is the most commonly used elastic modulus. It can be measured using the simplest mechanical test (i.e., the compression test, also called unconfined compression test) where samples are compressed between two planar surfaces (Table 1A). A displacement or a force is applied on the sample, and the force (F) delivered by the sample or the length difference (ΔL) is measured. If the sample surface (S) where the compression is applied and its initial thickness (L_0) are known, the axial stress (σ_y) and axial strain (ε_y) can be deduced. The Young's modulus (E) is given by the σ_y to ε_y ratio. The Young's modulus values increase proportionally with the sample stiffness. The Young's modulus of AC can also be calculated in tension using the traction test. Traction is generally applied in the lateral direction because it results from AC deformation during in vivo loading (Table 1B). The Young's modulus can also be measured using an indentation test at the millimetric scale (Table 1D).[7,76,77] Due to the

high increase in contact area during the indentation test, a specific equation, depending on the tip shape, is needed. For spherical indenters, the equation is given in Table 1D.

The Poisson's ratio characterizes the sample compressibility (ν) and is obtained by relating the opposite of the lateral strain ($-\varepsilon_x$) to the axial strain (ε_y), measured using a compression or a traction test. For example, the lateral strain (ε_y, Table 1A) is calculated by measuring the difference of the sample lateral size (Δl, the diameter for a disk) before and after compression. A compressible sample (when $\nu = 0$) does not display lateral expansion during axial compression, but its volume changes. The volume of an incompressible sample (when $\nu = 0.5$) does not change under compression, and the extension in lateral directions offsets the axial compression. Conversely, auxetic tissues (when $\nu < 0$) exhibits a lateral shrinkage during axial compression.

The AC aggregate modulus characterizes the matrix stiffness, especially in confined compression. Upon confined compression, water and proteoglycans are the major components that contribute to the mechanical strength (Table 1C). The sample is compressed in a cylindrical chamber by a rigid porous disk with an adjusted diameter to prevent lateral expansion. The aggregate modulus can be determined by relating the axial strain (ε_y) to the axial stress (σ_y) and the Poisson's ratio is equal to zero.

AC shear modulus is evaluated with shear tests (Table 1E). The AC sample is placed between two planar surfaces. A low axial strain is applied to ensure the contact between the sample and both surfaces, and then the upper surface is laterally displaced. The stress (σ_y) applied is deduced from the force (F) and the surface of application (S). Then, the strain is calculated as the ratio between the displacement of the upper surface (Δl) and the initial sample thickness (L_0). The shear modulus is determined as the ratio between stress and strain, like for the Young's modulus.

In addition to the Poisson's ratio, only one of these three parameters (Young's modulus, aggregate modulus, shear modulus) is needed to completely characterize the elasticity of a material for small deformations when it is considered isotropic. These three parameters differ in the direction of the solicitation (axial or lateral) or in the boundary conditions (confined or unconfined) of the system.

3.2.2 | Pseudo-elastic properties of native human AC

Many studies described the elastic properties of OA and healthy human AC at the millimetric scale (i.e., the tissue scale) (see Table 2 for selected studies). At equilibrium, the elastic modulus of healthy AC ranges from 250 kPa to 3 MPa in compression and from 7 to 13 MPa in traction. AC is considered as a soft tissue compared with bone where the Young's modulus is 17 GPa for femur, for example.[85,86] It has to be noted that the Young's modulus values obtained in compression, where proteoglycans and water are the main contributors, are smaller than those obtained in tension, where the response is related to COL II fibrils which are stiffer. Besides differences among mechanical tests, the Young's modulus value diversity can be explained also by the joint under study and the low to high weight-bearing area.[77] As proteoglycans resist to the compressive load and collagen fibrils resist to AC lateral expansion and swelling, the compressive modulus is higher in high weight-bearing areas while the tensile modulus is higher in low weight-bearing areas.[77,87] Moreover, it should be kept in mind that the pre-strain state before the mechanical test influences the equilibrium stiffness due to AC non-linear elasticity in the toe-region (see non-linear behavior, Section 3.2.3). The Poisson's ratio of healthy AC generally ranges from 0.14 to 0.18, indicating a compressible behavior. In OA, all AC elastic properties decrease due to proteoglycans loss, water content increase, and collagen fibrillation.[5,7]

3.2.3 | Variation in AC pseudo-elastic properties in function of the depth, direction, and deformation state

The elastic moduli determined using AC biopsies and one simple mechanical test are global measurements that do not fully represent AC complex mechanical behavior. Some studies indicate that more specific methods and complex models are needed to precisely understand and characterize AC elastic nature.

The first observation is AC non-linear elastic behavior: stiffness increases with the load amplitude when compressed, stretched or sheared (Figure 2A, dotted line). A J-shaped stress–strain curve is often observed and this indicates that the elastic behavior non-linearity is more pronounced at small strain values, within the toe-region (Figure 2A, dashed line).[5,72,80,88] As the elastic modulus is the stress–strain curve slope, the elastic modulus determined at a low strain value is much lower than at a higher strain value ($E_{0\%}$ and $E_{10\%}$ in Figure 2A, Table 2). Several hyperelastic models can be used to properly describe such non-linear behavior.[89,90]

The elastic moduli also vary in function of the directions and zones at the millimetric scale. During unconfined compression of AC disks, the amplitude of radial strains depends on their direction compared with that of the split line. At the AC biopsy surface, the initial circular shape becomes elliptic with less strain in the split line direction.[8,78] Unconfined and confined compression tests of AC biopsies that include the middle and deep zones (Figure 1) give higher Young's modulus and aggregate modulus values, respectively, in the tangential direction than in the perpendicular direction to the AC surface[72] (Table 2). Collagen fibrils, which resist to tension only, increase the Young's modulus of AC when compression is applied perpendicularly to their direction. Indentation tests showed that the Young's modulus and aggregate modulus values increase with depth. A progressive increase of the aggregate modulus value, from 20 ± 3 kPa (superficial layer) to 6.44 ± 1.02 MPa (calcified zone) was observed using a spherical tip of 500 µm diameter in the lateral direction of the AC slice.[76] A similar increase of the Young's modulus and aggregate modulus in function of the zone was also observed using unconfined and confined compression tests in the axial direction.[47,67] Moreover, compressibility is lower in the middle zone ($\nu \approx 0.4$), where the COL II fibril network is slacker, compared with the superficial and deep zones

TABLE 2 Mechanical properties of human articular cartilage measured at the millimetric scale

Technique	Sample	Organ state (normal/OA)	Site of characterization	Elastic moduli				Poro or visco-elastic parameters			Reference
				E_{eq} (kPa)	E_{dyn} (kPa)	ν	H_{a-eq} (kPa)	K (m^4/Ns)	μ (kPa.s)	τ (s)	
Unconfined compression	Femoral head			250–500		0.15–0.3					Boschetti[4]
	Femoral head			1640 ± 340		0.14 ± 0.09					Démarteau[78]
	Femoral head	Normal OA		450–700 100–300				$0.1–1 \times 10^{-14}$ $1–3 \times 10^{-14}$			Boshetti and Peretti[5]
	Femoral condyle or tibial plateau	Normal OA									Robinson[8]
	Knee: middle and deep zones		Perp. To AC surface Tang. To AC surface	581 ± 168 854 ± 348		0.158 ± 0.148 0.180 ± 0.046					Jurvelin[72]
Confined compression	Lateral facet of patella						790 ± 360	$0.47 \pm 0.36 \times 10^{-14}$			Armstrong and Mow[79]
	Femoral head						250–500	$0.15–0.35 \times 10^{-13}$			Boschetti[4]
	Femoral head		High deformation (0.1)				2220 ± 650	$1.1 \pm 0.6 \times 10^{-15}$			Démarteau[78]
	Humeral head and glenoid		Low deformation (0) High deformation (0.16)				1400 ± 60 1740 ± 70				Huang[80]
	Knee: middle and deep zones		Perp. To AC surface Tang. To AC surface				845 ± 383 1237 ± 486	$3–39 \times 10^{-15}$ $3–15 \times 10^{-15}$			Jurvelin[72]
	Femoral head		All sites 0–125 µm from AC surface 1.25–1.5 mm from AC surface				3000 ± 370 1160 ± 200 7750 ± 1450				Chen[67]
Traction	Humeral head and glenoid		Low deformation (0) High deformation (0.16)	4320 ± 2980 33,900 ± 26,770							Huang[80]
	Femoral head	Normal OA		7000–13,000 2000–3000	12,000–19,000 2000–5000						Boschetti and Peretti[5]
Indentation	Distal femoral head			606 ± 145				$1.50 \pm 0.37 \times 10^{-15}$			Athanasiou[77]
	Femoral head	Normal OA		1800 500	10,900 3400	0.47 0.47			218,700 36,000	16.7 9.0	Richard[7]
	Tibial plateau	Normal OA (OARSI 4)	Perp. To AC surface	1190 ± 560 210 ± 150	2000–90,000 600–35,000			$1.19 \pm 0.33 \times 10^{-15}$ $20.9 \pm 20.3 \times 10^{-15}$			Ebrahimi[81]
	Tibial plateau	Normal OA (OARSI 4)	Perp. To AC surface Fiber modulii (at fiber scale)	$100–450 \times 10^{+3}$ $100–300 \times 10^{+3}$				$0–2 \times 10^{-12}$ $2–20 \times 10^{-12}$			Moo[82]
			Superficial zone	20 ± 3							Antons[76]

(Continues)

TABLE 2 (Continued)

Technique	Sample	Organ state (normal/OA)	Site of characterization	Elastic moduli				Poro or visco-elastic parameters			Reference
				E_{eq} (kPa)	E_{dyn} (kPa)	ν	H_{a-eq} (kPa)	K (m^4/Ns)	μ (kPa.s)	τ (s)	
	Posterior femoral condyle		Calcified zone	6440 ± 1020							
Shear	Tibial plateau		0–500 μm from AC surface	400–1000 (G*)							Buckley[83]
			>500 μm from AC surface	1000–4000 (G*)							
	Talus and femoral condyle			100–6000 (G*)							Henak[84]

Note: The Young's modulus (E) and aggregate modulus (H_a) are determined at the articular cartilage equilibrium (E_{eq} and H_{a-eq}), when the tissue had the time to creep or relax, or during the load or immediately after its application (E_{dyn}), when the tissue shows an apparent modulus linked to its elasticity and viscous behaviors. The shear dynamic modulus (G^*) is measured during cyclic loading. Compressibility is characterized by the Poisson's ratio (ν). When time-dependent behaviors are taken into account, the permeability (k), viscosity (μ) and relaxation time (τ) are evaluated.

($\nu < 0.1$ and $\nu \approx 0.15$, respectively).[47] Conversely, mechanical characterization in tension of AC strips or biopsies from the superficial to the deep zone showed a decrease in stiffness because COL II fibrils are not parallel to the articular surface with depth and resist less to tensile constraints.[80,91]

3.2.4 | Variation in pseudo-elastic properties at different scales

At the microscale level (the cell scale), AC anisotropy and heterogeneity can be investigated at different depths and in different zones around the cells. AFM allows instrumented indentation at the microscale using a borosilicate microsphere of 5 μm in diameter (Table 1F). These indentation tests can determine the Young's modulus in different zones at different distance from the cells. The use of a micrometric spherical tip ensures that the mechanical characterization gives information on the mechanical rigidity at the cell scale. In different animal AC biopsies, this method revealed that the ECM superficial and deep zones are stiffer in the direction of COL II fibrils, whereas the middle zone exhibits subtle anisotropy.[40,51,92] The surface is subjected to more stress in the split line direction, while the deep zone is subjected to axial compression. Special attention must be paid to the indentation rate used for microscopic indentation tests. Indeed, when the indentation rate is high, stiffness increases with AC depth. Conversely, when the indentation rate is low, stiffness decreases.[51,68,92] When the indentation rate is high, fluid does not have the time to flow, and the fluid pressure is the main reaction to compression forces. When the indentation rate is low, the fluid movements do not influence much the compression reaction force and ECM stiffness is measured.[51] A decrease in the elastic modulus of the ECM with depth was observed and is related to the stiffness of COL II and proteoglycans fibrils ($E_{COL} = 384 \pm 50$ kPa, $E_{PG} = 22.3 \pm 1.5$ kPa) and their depth-dependent concentration.[93] Of note, the elastic moduli of the ECM (away from the cells) estimated at the micrometric and the millimetric scale are different (1–500 kPa vs. 300 kPa–10 MPa) (Tables 2, 3). Structural studies with high resolution imaging techniques and relevant numerical or theoretical models are needed to explain these differences.[97,98]

Microscale measurements can be used to evaluate the stress perceived by chondrocytes (Table 3). AFM showed that the pericellular matrix, which surrounds chondrocytes (Section 3.1), is softer than the interterritorial matrix.[95] Moreover, in the pericellular matrix, a positive gradient of the elastic modulus from the chondrocytes has been associated with a positive gradient of fluorescently labeled type VI collagen fibers and a negative gradient of perlecan.[40] The stiffness is higher in the territorial matrix thanks to the assembly of COL II fibrils, and reaches its maximum in the interterritorial matrix where COL II fibrils are highly organized.[9,99] This stiffness gradient could play a role in protecting chondrocytes against huge strain or stress, but also in initiating mechanotransduction signals. AFM has been also used to measure the cell stiffness and revealed that the Young's modulus of chondrocytes and mesenchymal stromal cells is 2 or 3 orders of

TABLE 3 Mechanical properties of human articular cartilage, chondrons, and chondrocytes at the microscopic scale

Technique	Organ	Organ state (normal/OA)	Site of characterization	Cell	Elastic moduli		Poro-elastic parameters	Reference
					E_{eq} (kPa)	E_{dyn} (kPa)	k (m^4/Ns)	
Indentation (AFM)	Femoral head		Cell	Spherical chondrocytes	0.45 ± 0.42			Darling[94]
			Cell	Spherical MSC	0.52 ± 0.60			
			Cell	Spherical chondrocytes	1.0 ± 1.6			
			Cell	Spread MSC	2.3 ± 2.1			
	Femoral condyle	Normal	ECM			306 ± 133		Darling[95]
			PCM			104 ± 51		
	Femoral condyle	Normal	ECM		491 ± 112			Wilusz[9]
		Normal	PCM		137 ± 22			
		OA	ECM		270 ± 76			
		OA	PCM		96 ± 16			
Micropipette aspiration	Femoral head	Normal	PCM; Superficial layer	Chondrocytes and chondrons	68.9 ± 18.9			Alexopoulos[2]
		OA	PCM; Superficial layer		39.1 ± 19.6			
		Normal	PCM; Deep layer		62.0 ± 30.5			
		OA	PCM; Deep layer		43.9 ± 23.0			
	Femoral head	Normal	PCM	Chondrocytes and chondrons	38.7 ± 16.2		4.19 ± 3.78 × 10^{-17}	Alexopoulos[3]
		OA	PCM		23.5 ± 12.9		10.2 ± 9.38 × 10^{-17}	
	Knee and hips		Cell	Chondrocytes in suspension in alginate	0.24 ± 0.11		4.2 × 10^{-15}	Trickey[96]
	Knees, hips, ankles, and elbows	Normal	Cell	Chondrocytes in suspension in alginate	0.65 ± 0.63			Jones[6]
		OA			0.67 ± 0.86			

Note: The Young's modulus (E) is determined at the equilibrium (E_{eq}), when the sample had the time to creep or relax, or during the load, or immediately after its application (E_{dyn}), when the sample shows the apparent modulus linked to its elasticity and viscous behaviors. Compressibility is characterized by the Poisson's ratio (v). When time-dependent behaviors are taken into account, permeability (k) is evaluated.

magnitude lower than that of the pericellular matrix when cells were spread or spherical, respectively.[94,95] Of note, similar values for the mechanical properties of chondrocytes, mesenchymal stromal cells, and pericellular matrix were obtained (Table 3) with the micropipette aspiration technique that is widely used to evaluate the cell mechanical properties (Table 1G). The Young's modulus is decreased in OA pericellular matrix, but not in OA chondrocytes.[2,3,6]

3.2.5 | Elasticity limit and failure

Analysis of knee arthroscopies demonstrated that overloading during day living activity or sport participation induces AC lesions, such as localized, osteochondral and chondral lesions, diffuse OA or osteochondritis dissecans.[100] In case of extreme strain, COL II fibrils snap and the disrupted network threatens the tissue integrity. Extreme AC behavior has been studied by applying high stress in compression or traction.[91,101,102] Upon fiber disruption, the force delivered by AC for a given displacement decreases, hysteresis increases due to higher energy loss, and residual deformations remain after loading.[102] The failure strain can be called "yield point" (i.e., elasticity limit) because part of the reversible tissue deformation disappears and the initial tissue shape cannot be recovered. For example, a failure strain of 113.8% ± 25.1% in tension and 30% ± 7% in compression has been measured in bovine AC samples using an indenter of 7 mm in diameter.[101,102] AC lesions reduce the tissue mechanical properties and promote chronic diseases. Finally, some efforts have been made to predict the impact-induced AC fissuring, but the mechanisms of AC fracture remain difficult to understand.[84,103–106] A cartilage injury may be the result of an impact that exceeded the tissue failure strain

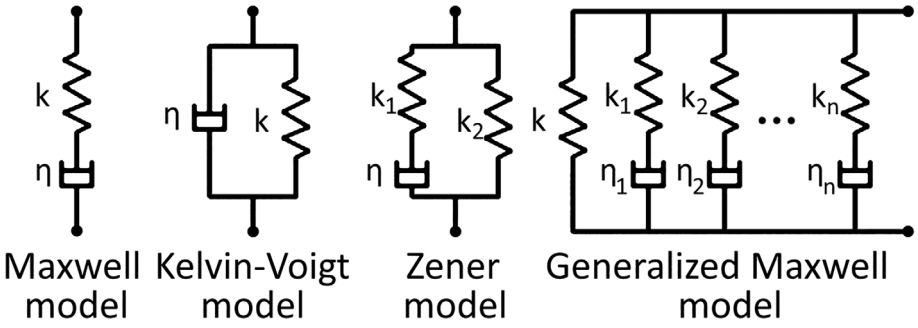

FIGURE 4 Constitutive models of viscoelasticity. Viscoelastic models are composed of purely elastic springs (to consider the material elasticity) and purely viscous dampers (to consider the energy dissipation). Springs are characterized by their stiffness (k), and dampers by their viscosity (η)

or of an impact that has not altered the tissue structure but has led to chondrocyte death followed by progressive degradation.

3.3 | What can be learnt from more complex fiber-reinforced osmo-poroviscoelastic models of AC

AC *purely elastic* properties cannot describe AC capacity to dampen loads by dissipating mechanical energy. Only parameters that can influence AC time-dependent behaviors can be used to properly estimate this feature. AC viscoelastic, poroelastic or poroviscoelastic features can be characterized by considering flow-independent and/or flow-dependent behaviors. Some fiber-reinforced osmo-poroelastic models have been developed to understand, characterize and reproduce the complex mechanical behaviors of AC.[90]

3.3.1 | Viscoelastic characterization

Four basic viscoelastic models, based on combinations of elastic and viscous models, have been described (Figure 4).[107] Currently, the Zener and generalized Maxwell models are the most commonly used to describe the viscoelastic behavior of AC, pericellular matrix and chondrocytes.[7,94,96,108] The Zener model describes creep or stress relaxation and recovery compared with simpler models, such as the Maxwell and Kelvin-Voigt models.[90] The generalized Maxwell model takes into account several time constants due to several viscous elements. Other rheological models of viscoelastic materials that combine two or more of the four basic models have been described.[107]

By fitting experimental data from a creep or relaxation test to a numerical model, the sample viscosity, dynamic and equilibrium elastic modulus, and Poisson's ratio can be determined. Viscosity values of 218.7 and 36.0 MPa were measured in human normal and OA AC, respectively, using an indentation test.[7] In vivo measures at the organ scale, using MR images of the femoral cartilage thickness in healthy knee, show creep times under body weight of approximately 60 s.[24] The creep and relaxation times are typically 16.7 and 9.0 s for normal and OA AC biopsies, respectively. These parameters depend on the strain due to the non-linear AC behavior. At the cell scale, chondrocytes and pericellular matrix are frequently characterized using a viscoelasticity model.[94,96,108,109] The different values of creep and relaxation times reveal the multi-scale nature of AC.

AC viscoelasticity can also be assessed using cyclic loading. The dynamic modulus (E^*) is a complex modulus composed of a storage modulus (E'), the elastic part, and a loss modulus (E''), the viscous part. Cyclic loading at several frequencies showed an increase in these two moduli following logarithmic curves.[110,111] Upon unconfined compression of human biopsies at 1 and 88 Hz, the storage moduli were 31.9 and 43.3 MPa and the loss moduli were 5.3 and 8.5 MPa, respectively.[111] This shows that the dynamic modulus values measured in single loading, creep or relaxation tests or by cyclic loading should be considered with caution because they can be influenced by the loading rate. For AC, the order of magnitude of dynamic elastic moduli do not change with frequency; however, the equilibrium elastic modulus seem more suitable for study comparison.

Importantly, these viscoelastic models remain limited because they do not explicitly take into account the fluid flow that largely contributes to the cartilage relaxation and creep behaviors.[88] Moreover, methods to characterize the fluid capacity to flow within pores should allow improving the knowledge on mechanotransduction pathways.

3.3.2 | Poroelastic characterization

Poroelastic models are biphasic models in the AC field that take into account both the fluid and the solid phase. Their major interest is that they can take in account and characterize the time-dependent effects associated with the fluid flow in pores at the cell scale, particularly in creep and relaxation tests. The solid phase, which corresponds to the network of collagen fibrils, proteoglycans and water, can be considered as an elastic material.[47,58,64,112] The fluid phase is mostly considered as an incompressible viscous fluid. By fitting the experimental data from a creep or stress relaxation test to the numerical model, the sample hydraulic conductivity, the dynamic and equilibrium elastic moduli, and the Poisson's ratio can be determined. The hydraulic conductivity describes the fluid capacity to flow within the tissue and is influenced by the intrinsic permeability and the fluid viscosity and density. Most of the time, the intrinsic permeability is the estimated parameter and its value varies in function of the pore size and volume fraction of the solid phase.

Due to its composition and structure, AC permeability is heterogeneous, anisotropic and low (between 10^{-15} and 10^{-13} m^4/Ns) (Table 2). Moreover, permeability is lower in the superficial and deep zones than in the middle zone.[113] In the superficial zone, a packing

network of thin COL II fibrils offers more resistance to the flow.[113] In the middle zone, permeability increases due to the larger and less organized COL II fibrils and a similar concentration of proteoglycans. As proteoglycans are responsible for water retention and the porosity decrease, cartilage permeability decreases from the middle to the deep zone with the increase of proteoglycan concentration.[113] Moreover, permeability is anisotropic because the fluid flow is affected by the COL II fibril orientation.[112] In addition, during AC compression, permeability decreases in a non-linear manner due to the change in fibril orientation and the pore size decrease.[5,72] In the pericellular matrix, a permeability gradient is created by the distribution of COL VI fibers. Indeed, pore size is larger next to chondrocytes than in the territorial and interterritorial matrix regions.[114] The nutrient and waste exchanges around chondrocytes are facilitated by this organization. In OA, the proteoglycan loss and COL II fiber fibrillation increase the pore size and therefore permeability.[5] This facilitates the fluid flow during load and decreases the dynamic elastic modulus.

To take into account both the flow-independent and flow-dependent damping behaviors of AC, the solid phase can be represented as a viscoelastic material.[58,88,115] At the macroscopic scale, the poroviscoelastic model well reproduces the axial and lateral responses to an unconfined compression test because both flow-independent and flow-dependent behaviors are involved in the tissue response to loads.[88] Indeed, the first part of a creep test is mainly governed by the flow-independent mechanism, whereas the second part is mainly governed by the flow-dependent mechanism.[63] However, at the microscopic scale, only the flow-dependent mechanism seems to influence creep tests. At this scale, the fluid flow seems to contribute mainly to the energy dissipation compared with the few molecular rearrangements of the solid phase. Thus, a poroelastic model could be enough to describe AC time-dependent behavior.[64,116,117]

3.3.3 | Fiber-reinforced osmo-poroelastic models

The first poroviscoelastic models could not reproduce the cartilage anisotropic elastic behavior and its capacity to swell that both contribute to its complex mechanical response.

Fiber-reinforced poroelastic models, which consider a fluid phase and a porous solid phase (proteoglycans and the linked water) enriched in fibers, better describe AC behavior under unconfined compression and nanoindentation than those without fibers.[64,118] Fiber-reinforced poroelastic model have been essential to identify the role of COL II fibers and proteoglycans and the effect of their depletion on the tissue biomechanical behavior.[119,120] This approach well reproduces the behavior of normal AC biopsies or after collagen or proteoglycans depletion during a relaxation test in unconfined compression.[120] Loss of proteoglycans results in a greater decrease of the tissue equilibrium elastic modulus (−63% ± 27%) than of the dynamic (instantaneous state) elastic modulus (−17% ± 11%). Loss of collagen leads to a decrease of both dynamic and equilibrium elastic modulus (−68% ± 76% and −49% ± 12%). Simulations showed that the affected collagen network increases the pore size and facilitates the water flow. The links between proteoglycans and collagen fibers are destroyed and the pore size is increased. Collagen loss also leads to a loss of proteoglycans that decreases the equilibrium elastic modulus. Moreover, COL II fibers have a role in the equilibrium state by supporting the radial tension caused by axial compression. Finally, it seems that the proteoglycan content mainly influences the equilibrium state, whereas the collagen content mainly influences the transient state by changing the permeability.

COL II fibril distribution, orientation, and mechanical properties are taken into account in fibril-reinforced poroelastic models. Conversely, the proteoglycan chemo-mechanical properties, which are important for the equilibrium elastic modulus, are implicitly considered as part of the single solid phase. However, AC swelling behavior (Section 3.2.1) is considered as the main phenomenon to explain AC elasticity at the equilibrium state.[121] Thus, so-called triphasic models, which are poroelastic models with an additional ionic phase, consider advantageously AC swelling.[121,122] The used parameters are the salt concentration of the bathing solutions and proteoglycan fixed-charge density (FCD) because they influence the rate of osmotic pressure changes with dilatation.[121,123] The FCD is a molar concentration associated with a number of charges. In AC, FCD increases with depth and decreases with age in accordance with the proteoglycan concentration changes.[113] In human AC, MRI measurements were used to indirectly quantify FCD (0.18 ± 0.08 mEq/ml).[124] Strain was inversely correlated with the FCD and this finding experimentally confirmed the link between AC elastic moduli and the ability of FCD to induce osmotic pressure. A modeling study used FCD values ranging from 0 to 0.25 mEq/ml for the pericellular matrix and from 0.005 to 0.2 mEq/ml for chondrocytes.[125]

By using a fibril-reinforced osmo-poroelastic model, Wilson's group[122] could well represent AC behavior because the fit of different mechanical tests (unconfined and confined compression, and indentation) was validated. This model included (i) an incompressible linear elastic solid phase reinforced by a non-linear viscoelastic model for primary and secondary COL II fibrils, (ii) an incompressible fluid phase, and (iii) an ionic phase where the swelling pressure depends on the osmotic pressure and molecular extension. The tissue heterogeneity and anisotropy were described by adjusting the fibril density and orientation and the fluid fraction. AC non-linear response was described by the non-linear behavior of fibrils and FCD value that depends on the tissue deformation state. Thus, several parameters could be calculated: the Young's modulus and Poisson's ratio of the solid matrix, the elastic modulus and viscosity of fibers, the amounts of primary and secondary fibrils, the permeability and other material constants. This shows that models to accurately describe AC mechanical behavior can be created. These models help to decipher the role of each cartilage component, but at higher computational costs. However, the non-fibrillar matrix used in this model was incomplete in terms of depth-dependent stiffness, viscoelasticity and anisotropy, which was recently overcomed by Moo and colleagues.[81,82] Moo and colleagues' study suggest that rather than the intrinsic quality of the collagen fibers (which remained constant), early stages of OA disorganize collagen fibrous network. To be valuable, these complex models need to be initialized by setting several non-trivial parameters, such as the

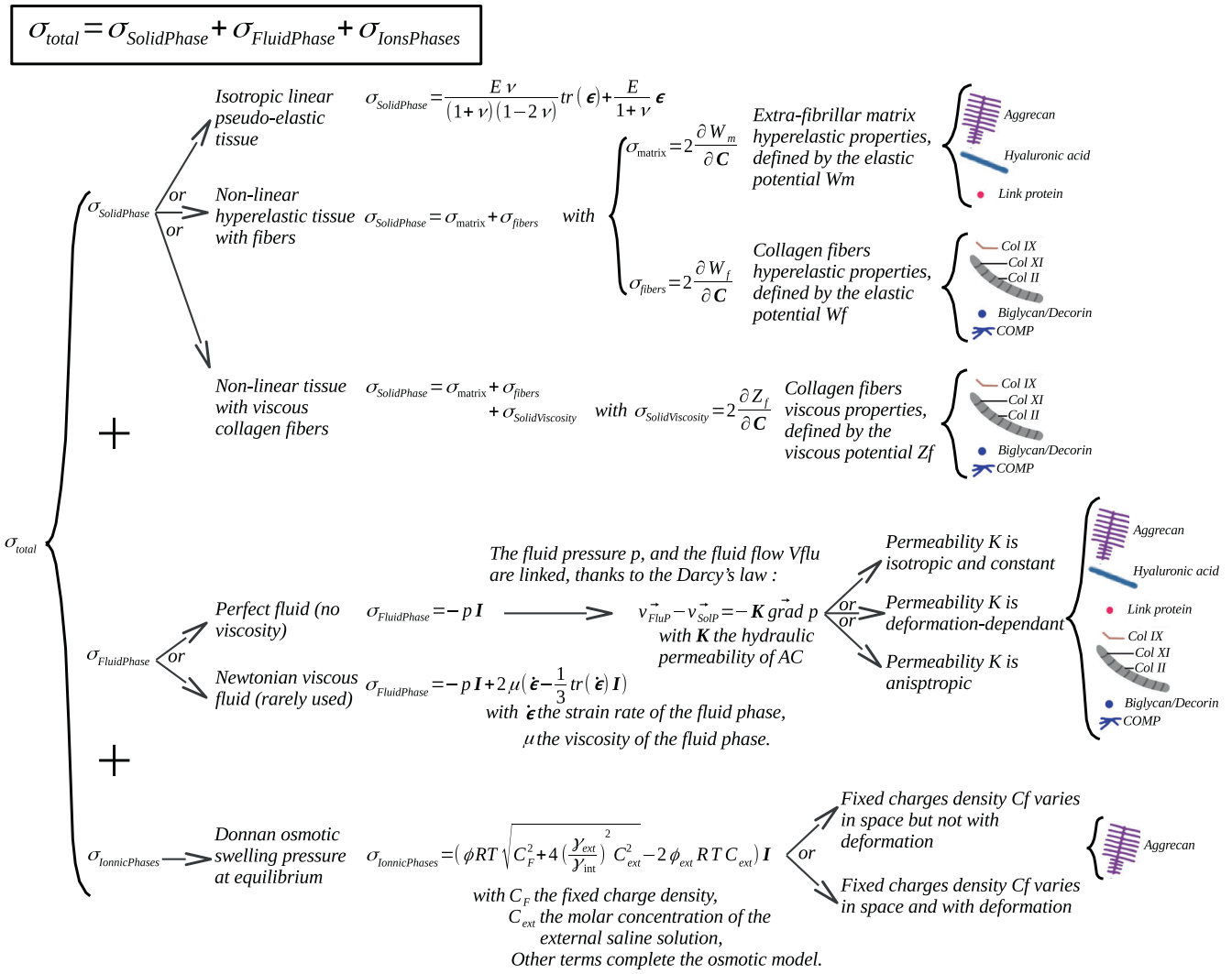

FIGURE 5 Decomposition of the constitutive laws acting in AC and link to micro-structural components. These constitutive laws describe the different behaviors that are mostly taken in account to model AC behavior in literature. σ_{total} is thus a simple summation of the solid phase stress tensor $\sigma_{\text{SolidPhase}}$ the fluid phase stress tensor $\sigma_{\text{FluidPhase}}$ together with the ionnic phase stress tensor $\sigma_{\text{IonnicPhases}}$. ε and C are measures of the deformation state of the sample (respectively the deformation tensor in linear elasticity and the right Cauchy-Green deformation tensor in hyper-elasticity). In addition to these constitutive laws, equilibrium equations, together with boundary equations and mass balance equations must be taken in account to fully describe a model of AC

fixed charge density, the fluid fraction and the fibril orientation. Moreover, huge datasets that take into account different mechanical loads are required for the validation of these models. In their review, Klika et al. describe such complex models to precisely reproduce AC behavior by taking into account its composition and structure.[126]

4 | RECOMMENDATIONS FOR THE BIOMECHANICAL CHARACTERIZATION OF CARTILAGE TISSUES

To summarize, increasingly sophisticated models have been developed to represent AC mechanical behavior as accurately as possible while respecting its composition and structure. The reviews of[90,126] and the recent works dealing with modeling AC and its characterization[82,127] outline that the stress acting within the media can be decomposed in an additive manner in three intuitive terms, one by phase (solid, fluid and ionic phases), as illustrated in Figure 5. For visco-poro-hyperelastic models reinforced with fibers the stress within the solid phase can itself be decomposed in three other main terms, one dealing with extra-fibrillar matrix, the second with the hyper-elasticity of fibers, and the last one with the viscosity of fibers.

For comparative studies or preliminary analyses, some hypotheses can be made to simplify the experimental design and data analysis, and one can use apparent moduli which refer to the so-called pseudo-elasticity concept. For instance, AC can be considered homogeneous, isotropic, and with linear pseudo-elasticity after the toe region (>10%

of strain). In case of using the pseudo-elasticity concept, particular attention should be paid to testing parameters, as apparent moduli will be affected by a change of most of the testing parameters, like strain rate, size of the specimen, saline bath concentration and temperature among others. As the proteoglycan content influences more the equilibrium elastic modulus than the dynamic elastic modulus,[120] both moduli could be evaluated using a purely elastic model and a creep or relaxation test, and proteoglycan production could be assessed in a non-destructive manner throughout the experiment. These first results could be completed by a destructive quantitative analysis of protein content at the study end to confirm the previous results. Measuring permeability in engineered cartilage constructs, which will be the focus of studies in the next years, is only possible using creep or stress relaxation tests, adequately completed by poroelastic or eventually poroviscoelastic models, to take in account the fluid flow. However, the models that best represent AC mechanical behavior, regardless of the chosen mechanical tests, are fiber-reinforced poroviscoelastic models, anisotropic poroviscoelastic models, or with an additional ionic phase to take in account swelling properties. Indeed, for the global analysis of the tissue, AC anisotropy, non-linear elasticity, non-linear permeability, non-homogeneous distribution of components and elasticity variations in function of the tissue depth must be taken into account.[82,128] Ultimately, multi-scale models, taking in account both depth variations and regional variation around cells would continue to increase our understanding of AC mechano-biological and bio-mechanical behavior.[53] However, this increases considerably the computation time and makes the model validation more difficult. Indeed, it is necessary to use or design adapted mechanical tests and in sufficient number to determine all the model parameters and their validity.

5 | CHALLENGES IN AC TISSUE ENGINEERING

Native AC has been described as a poroviscohyperelastic material characterized by component and structure gradients that are related to complex mechanical behaviors. The aim of AC engineering approaches is to generate functional AC to replace the injured tissues. However, engineered AC does not possess all the characteristics of native AC, and the current challenge is to provide sufficient bio-inspired media to copy the mechanical behaviors of native AC at its different scales and localizations.

5.1 | Mechanical parameters investigated in engineered tissues with and without scaffolds

The studies on the mechanical properties of tissue-engineered tissues, with or without cells, were selected when the biocompatibility of biomaterials with human chondrocytes or human mesenchymal stem cells was demonstrated (Table 4). Some studies on scaffold-free engineered tissues also were included.

Unconfined compression is the most used technique to evaluate the mechanical properties of a new engineered tissue. Confined compression, tension, shear or indentation tests are less frequently used, as already discussed in the review by Patel et al.[147] The dynamic and equilibrium elastic moduli of scaffold, hydrogel or scaffold-free engineered tissues are often under 250 kPa, indicating poor elastic moduli at the millimetric scale. After several weeks of culture during which cells secrete ECM components and remodel the construct, the equilibrium and dynamic elastic moduli increase or decrease, but they remain low compared with those of natural AC.[130,131,133,138,140,142,143,145] In this context, Lammi and colleagues discussed the challenges of cell colonization and the organization of the ECM in the constructs.[148] High cell concentration considerably increases the elastic moduli of hydrogels in compression.[131,133] Some scaffolds that are more structured than hydrogels display better elastic moduli.[137,144] Increasing the concentration of which component from 10% to 20% or creating interpenetrating polymer networks might improve the elastic moduli of hydrogels.[129,149] Moreover, the addition of COMP protein, involved in the ECM organization of the native AC, to a scaffold with rabbit BM-MSCs resulted in increased mechanical properties after implantation in vivo.[150] Interestingly, higher mechanical properties in tension and compression tests were obtained with scaffold-free engineered cartilage constructs.[139,141,146] Nevertheless, the high elastic modulus variability of scaffold-free constructs is influenced by cell culture conditions, cell type (BM-MSC, AT-MSC, chondrocytes) and cell origin.[139–141,146,151] Some scaffold-free constructs, consisting of human chondroprogenitor cells in hypoxic condition, display a good equilibrium elastic modulus compared with native AC and this is associated with increased proteoglycan and collagen production for 28 days.[141] However, their dynamic elastic modulus remains low compared with native AC. This can be explained by their lower collagen content than in native AC and the lack of collagen organization. Thus, the capacity of this new tissue to dampen forces will be limited.

To date, the primary objective of tissue engineering has been to provide cells with a biocompatible environment and to ensure sufficient apparent mechanical properties. Thus, most of the tested and described mechanical properties of engineered tissues only concern apparent moduli (Young's modulus or aggregate modulus) and do not take into account the features required for the proper tissue development and maintenance. Particular attention must now be paid to the elastic moduli at the tissue scale (heterogeneity, anisotropy, non-linearity) and also at the cell scale (lower elasticity moduli) as well as to other mechanical properties, such as permeability.

5.2 | Remaining challenges in reproducing AC mechanical behaviors

As already highlighted by Patel et al., a consistent and reproducible way to characterize the time-dependent and time-independent behaviors of new AC constructs should be standardized to allow the comparison of their mechanical parameters.[147] We suggest that complementary parameters also should be investigated.

TABLE 4 Mechanical properties of engineered human articular cartilage at the millimetric scale

				Elastic moduli					Failure	Poro or visco-elastic parameters			
Technique	Sample	Cell	Day of measure	E_{eq} (kPa)	E_{dyn} (kPa)	E' (kPa)	E^* (kPa)	H_{a-eq} (kPa)	Failure stress (kPa)	E'' (kPa)	$\tau_{1/2}$ (sec)	k (m^4/Ns)	Reference
Unconfined compression	15% Agarose hydrogels			480	870	3220 ± 347				140 ± 14			Roberts[129]
	15% PEG hydrogels			310	360	187 ± 27				0.0 ± 0.0			
	1% MeHA /MeGel hydrogel	hACh	D1 and D63	86	147 (at D63)		140 (at D63)		55 (at D63)				Levett[130]
	2% Agarose hydrogel 33–40 mcells/construct:	HACh	D28	50			250						Cigan[131]
	90 mcells/construct:	HACh	D28	254 ± 22			945 ± 65						
	5% Chitosan/1% Bovine ECM hydrogel				21.66 ± 0.41								Nasiri and Mashayekhan[132]
	1% MeHA hydrogel 20 mcells/ml	hMSC	D56	10			800						Kim[133]
	60 mcells/mL:	hMSC	D56	87			1250						
	2% Chitosan/0.5% hECM hydrogel				150 ± 10								Sivandzade and Mashayekhan[134]
	PLCL/Chitosan scaffold	hMSC	D0		128 ± 16.9								Yang[135]
		hMSC	D35		753.3 ± 210								
	7 and 11% porcine /ECM scaffold	hMSC	D0	4–35									Rowland[136]
		hMSC	D28	15–20									
	Silk/silk-CS scaffold			1050 (silk)									Zhou[137]
	Equin COL I scaffold	hMSC	D21	8.33 ± 3.28	9.42 ± 4.22						48.7 ± 11.7		Gullotta[138]
	Scaffold free	hMSC	D3, D5 and D7	788 ± 200 (at D3)									Bhumiratana[139]
	Scaffold free	hMSC	D28	37 ± 15	231 ± 25								Murphy[140]
		hACh	D28	13 ± 5	82 ± 36								
	Scaffold free	hACh	D28	3–200									Anderson[141]
		hAChP	D28	100–1000									
Confined compression	porcin ECM scaffold	hASC	D0 and D42					151 (at D42)				0.055×10^{-12}	Cheng[142]

TABLE 4 (Continued)

Technique	Sample	Cell	Day of measure	Elastic moduli					Failure	Poro or visco-elastic parameters			Reference
				E_{eq} (kPa)	E_{dyn} (kPa)	E' (kPa)	E^* (kPa)	H_{a-eq} (kPa)	Failure stress (kPa)	E'' (kPa)	$\tau_{1/2}$ (sec)	k (m^4/Ns)	
	porcin ECM scaffold	hACh	D7 and D28					21 (at D28)				0.0055×10^{-12}	Cheng[143]
Indentation	PLLA scaffolds (pore size variations)			3000–28,000									Tanaka[144]
Shear	Chitosan hydrogel	hACh	D14			9.6							Concaro[145]
			D28			14.6							
Traction	Scaffold free	hMSC	D14 and D21		5000 (at D21)				1320 ± 250 (at D21)				Ando[146]
	Scaffold free	hACh	D28		660 ± 251				292 ± 113				Murphy[140]

Note: These studies concerned engineered cartilage tissues with a scaffold, hydrogel, or without exogenous matrix and different human cell types (hACh: articular chondrocytes, hAChP: articular chondroprogenitors, hMSC: mesenchymal stem cells, hASC: adipose-derived mesenchymal stem cells). The tissues were mechanically characterized immediately or after several days of culture (*D*). The Young's modulus (*E*) and aggregate modulus (H_a) are determined at the articular cartilage equilibrium (E_{eq} and H_{a-eq}), when the tissue had the time to creep or relax, during the loading, or immediately after its application (E_{dyn}) when the tissue shows the apparent modulus linked to its elasticity and viscous behaviors. During cyclic loading, the dynamic modulus (E^*, G^*) or the storage modulus (E') and the loss modulus (E'') can be measured. Compressibility is characterized by the Poisson's ratio (ν). When time-dependent behaviors are taken in account, the permeability (k) and a relaxation half-life time ($\tau^{1/2}$) are evaluated.

First, even if it seems obvious, very few studies analyzed the failure stress or failure strain that must be estimated to minimize the risk of failure during in vivo solicitations. Overall, very few groups managed to develop a biomaterial that can sustain in vivo loads with proper elastic modulus.[137,140,144] An approximate failure strain of 30% in traction was found for scaffold-free constructs,[140,146] which is too small compared to what observed in bovine AC.[101] However, one of these studies showed that the tensile strength increases over time.[146]

Second, to our knowledge, only one group has studied the permeability of engineered AC tissue. Specifically, Cheng et al. showed that the permeability of their biomaterial remained 10 orders of magnitude higher than that of AC.[142,143] The lack of proper permeability in current constructs, even after cell seeding, seems to be a drawback that has not been taken into account in most of the biomaterials developed for AC replacement. The high permeability of engineered constructs for AC replacement alters the construct damping properties and the interstitial fluid flow. Changes in damping properties and in fluid flow affect the capacity of cartilage constructs to withstand high loading speeds and to optimize the cell phenotype, respectively.[152,153]

Third, the gradients of AC composition and structure play an important role in AC capacity to sustain different loads and in its homeostasis. This leads to AC heterogeneity and anisotropy that are rarely reproduced in tissue engineering. The increase in elastic moduli and the anisotropy changes with depth allow the AC to resist the compressions, tensions and shears that occur at its surface. An increase in elastic modulus has been achieved with at least two layers of hydrogel or a continuous gradient of composition, cross-linking, porosity, or cell density to induce the secretion of different ECM components; however, these tissues remain too soft and isotropic.[154–156] Similar gradients have been introduced in scaffolds that remain more rigid.[157] Anisotropy can be added by using fiber-reinforced hydrogels, by varying the pore structure, or by using additive manufacturing and by printing specific geometries.[158–160] As noted earlier, the mechanical behavior of engineered tissues has not been sufficiently tested at the tissue scale, using compression and shear tests for example, to determine their capacity to withstand different loads in joints and in different directions, where anisotropy is needed.

One of the major issues in AC tissue engineering is the supply of a biomaterial with sufficient mechanical properties for the implantation of the new tissue, while ensuring the cell differentiation and/or maintenance of the chondrocyte phenotype.[161] Indeed, the stiffness of the matrix on which cells are seeded influences their phenotype; however, the stiffness required at the AC tissue level is too important to promote the chondrocyte phenotype.[162,163] Currently, hydrogels display mechanical properties adapted for cells, with sometimes gradients of mechanical properties that allow obtaining the different chondrocyte phenotypes found in AC.[156,164] However, these hydrogels are too weak to sustain in vivo mechanical loads. On the other hand, stiffer scaffolds with mechanical properties adapted to in vivo loads promotes a hypertrophic phenotype because the matrix around the cells is too stiff (Table 4). It should be noted, however, that the tissue should not be too rigid either, as it would be difficult to position, would not be

mechanically stable and could cause damage to the resting cartilage and subchondral bone.[165] Two AC characteristics could be considered in future tissue engineering approaches: the gradient of mechanical properties from the pericellular to the interterritorial region, and AC composition and structure that generate mechanical properties 10 times lower at the cell scale than at the tissue scale, all zones and regions combined. Additive manufacturing techniques, such as electrospinning and 3D bioprinting, are interesting because they can build structures that closely mimic AC.[166,167] Better cell colonization and ECM organization were guided with a scaffold generated by additive manufacturing.[168] A combination of a strong structure and a softer hydrogel in which cells are embedded also could be a solution.[160] However, it will not be possible to validate these techniques and mimic these two characteristics without a more complete mechanical characterization of AC at the tissue and cell level.

In conclusion, additive manufacturing techniques are promising approaches for creating engineered cartilage with better properties. Gradients or layers with different composition or/and organization of biomaterials are needed to create new tissues with gradients of mechanical properties as found in the native tissue and to take into account the differences at the tissue and cell scale. Such approaches might help to overcome biomechanical issues concerning the balance between mechanical properties tailored to the tissue function and to the cell environment. However, the mechanical characterization of these tissues needs to be improved. Multi-creep or multi-relaxation tests in at least two configurations (for instance, compression and shear) are needed to evaluate the dynamic and equilibrium elastic moduli and the tissue permeability. Anisotropy can be assessed by analyzing the tissue mechanical properties in different directions. A simple test to non-reversible mechanical deformation can be used to determine the mechanical limit of the tissue. Finally, AFM allows evaluating the cell mechanical environment. Of note, this comprehensive analysis should be performed at several time points to monitor the engineered tissue development because cells can positively or negatively influence the tissue mechanical properties by remodeling their environment.

6 | CONCLUSION

The complex biomechanical behavior of AC is characterized by its non-linear elasticity, viscosity, permeability, compressibility, heterogeneity, and anisotropy. Several theoretical and numerical models have been developed to reproduce and study its mechanical behaviors. A key issue for AC mechanical characterization is the combination of an experimental setup to drive and measure mechanical solicitation with a model to specify the needed assumptions.

AC damping nature, related to its poroviscoelastic behavior, has focused much attention and several studies have outlined the importance of dissipation for AC engineering, both in vitro and in vivo.[169,170] Indeed, by finely tuning the damping and poroelastic properties of engineered tissues, mechanical stimulations should optimize the distribution of nutrients to cells throughout the tissue.

Another key feature of AC is the multi-scale nature of its mechanical behaviors. Due to its specific fibrous microstructure and spatial gradient around cells, AC exhibits low stiffness at the cell scale and relatively high stiffness at the tissue scale. This feature must be thoroughly investigated using multi-scale modeling and must be taken into account when developing new biomaterials.

The production of engineered cartilage tissue for transplantation requires many adjustments concerning cells, biomaterials, biological and biomechanical factors.[171] Reproducing AC mechanical behavior is one of them. This is a huge task. Numerical modeling can help to describe the mechanical behavior and quantify the mechanical parameters of native AC and also to model the mechanical behavior of engineered tissues and adjust their composition or micro-structural geometry.[172]

ACKNOWLEDGMENTS

We gratefully acknowledge funding support from the University of Montpellier, Inserm, Cartigen plateform and Occitanie region. This work benefitted from a French State grant managed by the French National Research Agency under the Investments for the Future programme (reference n°ANR-10-LABX-20). This work has received financial support from CNRS through the MITI interdisciplinary programs (AAP "Osez l'interdesciplinarité 2018", MoTiV Project).

DATA AVAILABILITY STATEMENT

Data sharing is not applicable to this article as no new data were created or analyzed in this study.

ORCID

Simon Le Floc'h https://orcid.org/0000-0001-7859-1515

REFERENCES

1. Sophia Fox AJ, Bedi A, Rodeo SA. The basic science of articular cartilage. *Sports Health*. 2009;1:461-468. doi:10.1177/1941738109350438
2. Alexopoulos LG, Haider MA, Vail TP, Guilak F. Alterations in the mechanical properties of the human chondrocyte pericellular matrix with osteoarthritis. *J Biomech Eng*. 2003;125:323-333.
3. Alexopoulos LG, Williams GM, Upton ML, Setton LA, Guilak F. Osteoarthritic changes in the biphasic mechanical properties of the chondrocyte pericellular matrix in articular cartilage. *J Biomech*. 2005;38:509-517. doi:10.1016/j.jbiomech.2004.04.012
4. Boschetti F, Pennati G, Gervaso F, Peretti GM, Dubini G. Biomechanical properties of human articular cartilage under compressive loads. *Biorheology*. 2004;41:159-166.
5. Boschetti F, Peretti GM. Tensile and compressive properties of healthy and osteoarthritic human articular cartilage. *Biorheology*. 2008;45:337-344. doi:10.3233/BIR-2008-0479
6. Jones WR, Ping Ting-Beall H, Lee GM, Kelley SS, Hochmuth RM, Guilak F. Alterations in the Young's modulus and volumetric properties of chondrocytes isolated from normal and osteoarthritic human cartilage. *J Biomech*. 1999;32:119-127. doi:10.1016/S0021-9290(98)00166-3
7. Richard F, Villars M, Thibaud S. Viscoelastic modeling and quantitative experimental characterization of normal and osteoarthritic human articular cartilage using indentation. *J Mech Behav Biomed Mater*. 2013;24:41-52. doi:10.1016/j.jmbbm.2013.04.012
8. Robinson DL, Kersh ME, Walsh NC, Ackland DC, de Steiger RN, Pandy MG. Mechanical properties of normal and osteoarthritic human articular cartilage. *J Mech Behav Biomed Mater*. 2016;61:96-109. doi:10.1016/j.jmbbm.2016.01.015

9. Wilusz RE, Zauscher S, Guilak F. Micromechanical mapping of early osteoarthritic changes in the pericellular matrix of human articular cartilage. *Osteoarthr Cartil*. 2013;21:1895-1903. doi:10.1016/j.joca.2013.08.026
10. Huey DJ, Hu JC, Athanasiou KA. Unlike bone, cartilage regeneration remains elusive. *Science*. 2012;338:917-921. doi:10.1126/science.1222454
11. Du D, Hsu P, Zhu Z, Zhang C. Current surgical options and innovation for repairing articular cartilage defects in the femoral head. *J Orthop Transl*. 2020;21:122-128. doi:10.1016/j.jot.2019.06.002
12. DuRaine GD, Brown WE, Hu JC, Athanasiou KA. Emergence of scaffold-free approaches for tissue engineering musculoskeletal cartilages. *Ann Biomed Eng*. 2015;43:543-554. doi:10.1007/s10439-014-1161-y
13. Huang BJ, Hu JC, Athanasiou KA. Cell-based tissue engineering strategies used in the clinical repair of articular cartilage. *Biomaterials*. 2016;98:1-22. doi:10.1016/j.biomaterials.2016.04.018
14. Kon E, Filardo G, Roffi A, Andriolo L, Marcacci M. New trends for knee cartilage regeneration: from cell-free scaffolds to mesenchymal stem cells. *Curr Rev Musculoskelet Med*. 2012;5:236-243. doi:10.1007/s12178-012-9135-x
15. Kon E, Perdisa F, Filardo G, Andriolo L, Tentoni F, Marcacci M. Biomaterials for osteochondral reconstruction. *Dev Insights Cartil Repair*. 2014;99-108. doi:10.1007/978-1-4471-5385-6_6
16. Zumwalt M, Reddy AP. Stem cells for treatment of musculoskeletal conditions—orthopaedic/sports medicine applications. *Biochim Biophys*. 1866;2020:165624. doi:10.1016/j.bbadis.2019.165624
17. Alford JW, Cole BJ. Cartilage restoration, part 1: basic science, historical perspective, patient evaluation, and treatment options. *Am J Sports Med*. 2005;33:295-306. doi:10.1177/0363546504273510
18. Bergmann G, Deuretzbacher G, Heller M, et al. Hip contact forces and gait patterns from routine activities. *J Biomech*. 2001;34:859-871. doi:10.1016/S0021-9290(01)00040-9
19. Eckstein F, Lemberger B, Gratzke C, et al. In vivo cartilage deformation after different types of activity and its dependence on physical training status. *Ann Rheum Dis*. 2005;64:291-295. doi:10.1136/ard.2004.022400
20. Hodge WA, Fijan RS, Carlson KL, Burgess RG, Harris WH, Mann RW. Contact pressures in the human hip joint measured in vivo. *Proc Natl Acad Sci*. 1986;83:2879-2883.
21. Kutzner I, Heinlein B, Graichen F, et al. Loading of the knee joint during activities of daily living measured in vivo in five subjects. *J Biomech*. 2010;43:2164-2173. doi:10.1016/j.jbiomech.2010.03.046
22. Liu F, Kozanek M, Hosseini A, et al. In vivo tibiofemoral cartilage deformation during the stance phase of gait. *J Biomech*. 2010;43:658-665. doi:10.1016/j.jbiomech.2009.10.028
23. Bingham JT, Papannagari R, van de Velde SK, et al. In vivo cartilage contact deformation in the healthy human tibiofemoral joint. *Rheumatology*. 2008;47:1622-1627. doi:10.1093/rheumatology/ken345
24. Hosseini A, van de Velde SK, Kozanek M, et al. In-vivo time-dependent articular cartilage contact behavior of the tibiofemoral joint. *Osteoarthr Cartil*. 2010;18:909-916. doi:10.1016/j.joca.2010.04.011
25. Li G, Wan L, Kozanek M. Determination of real-time in-vivo cartilage contact deformation in the ankle joint. *J Biomech*. 2008;41:128-136. doi:10.1016/j.jbiomech.2007.07.006
26. Prekasan D, Saju KK. Review of the tribological characteristics of synovial fluid. *Procedia Technol*. 2016;25:1170-1174. doi:10.1016/j.protcy.2016.08.235
27. Zhou ZR, Jin ZM. Biotribology: recent progresses and future perspectives. *Biosurface Biotribol*. 2015;1:3-24. doi:10.1016/j.bsbt.2015.03.001
28. Riesle J, Hollander AP, Langer R, Freed LE, Vunjak-Novakovic G. Collagen in tissue-engineered cartilage: types, structure, and crosslinks. *J Cell Biochem*. 1998;71:313-327. doi:10.1002/(SICI)1097-4644(19981201)71:3<313::AID-JCB1>3.0.CO;2-C
29. Sherman VR, Yang W, Meyers MA. The materials science of collagen. *J Mech Behav Biomed Mater*. 2015;52:22-50. doi:10.1016/j.jmbbm.2015.05.023
30. Carney SL, Muir H. The structure and function of cartilage proteoglycans. *Physiol Rev*. 1988;68:858-910. doi:10.1152/physrev.1988.68.3.858
31. Bouhrara M, Reiter DA, Sexton KW, Bergeron CM, Zukley LM, Spencer RG. Clinical high-resolution mapping of the proteoglycan-bound water fraction in articular cartilage of the human knee joint. *Magn Reson Imaging*. 2017;43:1-5. doi:10.1016/j.mri.2017.06.011
32. Reiter DA, Roque RA, Lin P-C, et al. Mapping proteoglycan-bound water in cartilage: improved specificity of matrix assessment using multiexponential transverse relaxation analysis. *Magn Reson Med*. 2011;65:377-384. doi:10.1002/mrm.22673
33. Ameye L, Young MF. Mice deficient in small leucine-rich proteoglycans: novel in vivo models for osteoporosis, osteoarthritis, Ehlers-Danlos syndrome, muscular dystrophy, and corneal diseases. *Glycobiology*. 2002;12:107R-116R. doi:10.1093/glycob/cwf065
34. Douglas T, Heinemann S, Bierbaum S, Scharnweber D, Worch H. Fibrillogenesis of collagen types I, II, and III with small leucine-rich proteoglycans decorin and biglycan. *Biomacromolecules*. 2006;7:2388-2393. doi:10.1021/bm0603746
35. Roughley PJ. The structure and function of cartilage proteoglycans. *Eur Cell Mater*. 2006;12:92-101. doi:10.22203/ecm.v012a11
36. Wiberg C, Klatt AR, Wagener R, et al. Complexes of matrilin-1 and biglycan or decorin connect collagen VI microfibrils to both collagen II and aggrecan. *J Biol Chem*. 2003;278:37698-37704. doi:10.1074/jbc.M304638200
37. Knudson CB, Knudson W. Cartilage proteoglycans. *Semin Cell Dev Biol*. 2001;12:69-78. doi:10.1006/scdb.2000.0243
38. Kvist AJ, Nyström A, Hultenby K, Sasaki T, Talts JF, Aspberg A. The major basement membrane components localize to the chondrocyte pericellular matrix—a cartilage basement membrane equivalent? *Matrix Biol*. 2008;27:22-33. doi:10.1016/j.matbio.2007.07.007
39. Vincent TL, McLean CJ, Full LE, Peston D, Saklatvala J. FGF-2 is bound to perlecan in the pericellular matrix of articular cartilage, where it acts as a chondrocyte mechanotransducer. *Osteoarthr Cartil*. 2007;15:752-763. doi:10.1016/j.joca.2007.01.021
40. Wilusz RE, Defrate LE, Guilak F. A biomechanical role for perlecan in the pericellular matrix of articular cartilage. *Matrix Biol J Int Soc Matrix Biol*. 2012a;31:320-327. doi:10.1016/j.matbio.2012.05.002
41. Gilbert SJ, Bonnet CS, Blain EJ. Mechanical cues: bidirectional reciprocity in the extracellular matrix drives mechano-signalling in articular cartilage. *Int J Mol Sci*. 2021;22:13595. doi:10.3390/ijms222413595
42. Larsson T, Sommarin Y, Paulsson M, et al. Cartilage matrix proteins. A basic 36-kDa protein with a restricted distribution to cartilage and bone. *J Biol Chem*. 1991;266:20428-20433.
43. Benninghoff A. Form und Bau der Gelenkknorpel in ihren Beziehungen zur Funktion. *Z Für Zellforsch Mikrosk Anat*. 1925;2:783-862. doi:10.1007/BF00583443
44. Hunziker EB, Michel M, Studer D. Ultrastructure of adult human articular cartilage matrix after cryotechnical processing. *Microsc Res Tech*. 1997;37:271-284. doi:10.1002/(SICI)1097-0029(19970515)37:4<271::AID-JEMT3>3.0.CO;2-O
45. Matcher SJ. What can biophotonics tell us about the 3D microstructure of articular cartilage? *Quant Imaging Med Surg*. 2015;5:143-158. doi:10.3978/j.issn.2223-4292.2014.12.03
46. Lammi PE, Lammi MJ, Hyttinen MM, Panula H, Kiviranta I, Helminen HJ. Site-specific immunostaining for type X collagen in noncalcified articular cartilage of canine stifle knee joint. *Bone*. 2002;31:690-696. doi:10.1016/S8756-3282(02)00904-3

47. Laasanen MS, Töyräs J, Korhonen RK, et al. Biomechanical properties of knee articular cartilage. *Biorheology*. 2003;40:133-140.
48. Luo Y, Sinkeviciute D, He Y, et al. The minor collagens in articular cartilage. *Protein Cell*. 2017;8:560-572. doi:10.1007/s13238-017-0377-7
49. Thomas JT, Ayad S, Grant ME. Cartilage collagens: strategies for the study of their organisation and expression in the extracellular matrix. *Ann Rheum Dis*. 1994;53:488-496.
50. Youn I, Choi JB, Cao L, Setton LA, Guilak F. Zonal variations in the three-dimensional morphology of the chondron measured in situ using confocal microscopy. *Osteoarthr Cartil*. 2006;14:889-897. doi:10.1016/j.joca.2006.02.017
51. McLeod MA, Wilusz RE, Guilak F. Depth-dependent anisotropy of the micromechanical properties of the extracellular and Pericellular matrices of articular cartilage evaluated via atomic force microscopy. *J Biomech*. 2013;46:586-592. doi:10.1016/j.jbiomech.2012.09.003
52. Gaytan F, Morales C, Reymundo C, Tena-Sempere M. A novel RGB-trichrome staining method for routine histological analysis of musculoskeletal tissues. *Sci Rep*. 2020;10:1-13. doi:10.1038/s41598-020-74031-x
53. Wang X, Neu CP, Pierce DM. Advances toward multiscale computational models of cartilage mechanics and mechanobiology. *Curr Opin Biomed Eng*. 2019;11:51-57. doi:10.1016/j.cobme.2019.09.013
54. Ebrahimi M, Turunen MJ, Finnilä MA, et al. Structure–function relationships of healthy and osteoarthritic human tibial cartilage: experimental and numerical investigation. *Ann Biomed Eng*. 2020;48:2887-2900. doi:10.1007/s10439-020-02559-0
55. Martínez-Moreno D, Jiménez G, Gálvez-Martín P, Rus G, Marchal JA. Cartilage biomechanics: a key factor for osteoarthritis regenerative medicine. *Biochim Biophys Acta (BBA) - Mol Basis Dis*. 2019;1865:1067-1075. doi:10.1016/j.bbadis.2019.03.011
56. Mixon A, Savage A, Bahar-Moni AS, Adouni M, Faisal T. An in vitro investigation to understand the synergistic role of MMPs-1 and 9 on articular cartilage biomechanical properties. *Sci Rep*. 2021;11:1-11. doi:10.1038/s41598-021-93744-1
57. Fung YC. *Biomechanics: Mechanical Properties of Living Tissues*. 2nd ed. Springer; 1993.
58. Huang C-Y, Soltz MA, Kopacz M, Mow VC, Ateshian GA. Experimental verification of the roles of intrinsic matrix viscoelasticity and tension-compression nonlinearity in the biphasic response of cartilage. *J Biomech Eng*. 2003;125:84-93. doi:10.1115/1.1531656
59. Wilson W, van Donkelaar CC, van Rietbergen R, Huiskes R. The role of computational models in the search for the mechanical behavior and damage mechanisms of articular cartilage. *Med Eng Phys*. 2005b;27:810-826. doi:10.1016/j.medengphy.2005.03.004
60. Mak AF. The apparent viscoelastic behavior of articular cartilage—the contributions from the intrinsic matrix viscoelasticity and interstitial fluid flows. *J Biomech Eng*. 1986;108:123-130. doi:10.1115/1.3138591
61. Han L, Dean D, Ortiz C, Grodzinsky AJ. Lateral nanomechanics of cartilage aggrecan macromolecules. *Biophys J*. 2007;92:1384-1398. doi:10.1529/biophysj.106.091397
62. Maier F, Drissi H, Pierce DM. Shear deformations of human articular cartilage: certain mechanical anisotropies apparent at large but not small shear strains. *J Mech Behav Biomed Mater*. 2017;65:53-65. doi:10.1016/j.jmbbm.2016.08.012
63. DiSilvestro MR, Zhu Q, Suh J-KF. Biphasic Poroviscoelastic simulation of the unconfined compression of articular cartilage: II—effect of variable strain rates. *J Biomech Eng*. 2000;123:198-200. doi:10.1115/1.1351887
64. Nia HT, Han L, Li Y, Ortiz C, Grodzinsky A. Poroelasticity of cartilage at the nanoscale. *Biophys J*. 2011;101:2304-2313. doi:10.1016/j.bpj.2011.09.011
65. Oloyede A, Flachsmann R, Broom ND. The dramatic influence of loading velocity on the compressive response of articular cartilage. *Connect Tissue Res*. 1992;27:211-224. doi:10.3109/03008209209006997
66. Park S, Hung CT, Ateshian GA. Mechanical response of bovine articular cartilage under dynamic unconfined compression loading at physiological stress levels. *Osteoarthr Cartil*. 2004;12:65-73. doi:10.1016/j.joca.2003.08.005
67. Chen AC, Bae WC, Schinagl RM, Sah RL. Depth- and strain-dependent mechanical and electromechanical properties of full-thickness bovine articular cartilage in confined compression. *J Biomech*. 2001;34:1-12. doi:10.1016/S0021-9290(00)00170-6
68. Park S, Costa KD, Ateshian GA, Hong K-S. Mechanical properties of bovine articular cartilage under microscale indentation loading from atomic force microscopy. *Proc Inst Mech Eng: H*. 2009;223:339-347. doi:10.1243/09544119JEIM516
69. Responte DJ, Natoli RM, Athanasiou KA. Collagens of articular cartilage: structure, function, and importance in tissue engineering. *Crit Rev Biomed Eng*. 2007;35:363-411.
70. Sun Y-L, Luo Z-P, Fertala A, An K-N. Stretching type II collagen with optical tweezers. *J Biomech*. 2004;37:1665-1669. doi:10.1016/j.jbiomech.2004.02.028
71. Beck EC, Barragan M, Tadros MH, Gehrke SH, Detamore MS. Approaching the compressive modulus of articular cartilage with a decellularized cartilage-based hydrogel. *Acta Biomater*. 2016;38:94-105. doi:10.1016/j.actbio.2016.04.019
72. Jurvelin JS, Buschmann MD, Hunziker EB. Mechanical anisotropy of the human knee articular cartilage in compression. *Proc Inst Mech Eng H*. 2003;217:215-219. doi:10.1243/095441103765212712
73. Kirchdoerfer T, Ortiz M. Data-driven computational mechanics. *Comput Methods Appl Mech Eng*. 2016;304:81-101.
74. Leygue A, Coret M, Réthoré J, Stainier L, Verron E. Data-based derivation of material response. *Comput Methods Appl Mech Eng*. 2018;331:184-196. doi:10.1016/j.cma.2017.11.013
75. Theret DP, Levesque MJ, Sato M, Nerem RM, Wheeler LT. The application of a homogeneous half-space model in the analysis of endothelial cell micropipette measurements. *J Biomech Eng*. 1988;110(3):190-199. doi:10.1115/1.3108430
76. Antons J, Marascio MGM, Nohava J, et al. Zone-dependent mechanical properties of human articular cartilage obtained by indentation measurements. *J Mater Sci Mater Med*. 2018;29:57. doi:10.1007/s10856-018-6066-0
77. Athanasiou KA, Rosenwasser MP, Buckwalter JA, Malinin TI, Mow VC. Interspecies comparisons of in situ intrinsic mechanical properties of distal femoral cartilage. *J Orthop Res*. 1991;9:330-340. doi:10.1002/jor.1100090304
78. Démarteau O, Pillet L, Inaebnit A, Borens O, Quinn TM. Biomechanical characterization and in vitro mechanical injury of elderly human femoral head cartilage: comparison to adult bovine humeral head cartilage. *Osteoarthr Cartil*. 2006;14:589-596. doi:10.1016/j.joca.2005.12.011
79. Armstrong CG, Mow VC. Variations in the intrinsic mechanical properties of human articular cartilage with age, degeneration, and water content. *JBJS*. 1982;64:88-94.
80. Huang C-Y, Stankiewicz A, Ateshian GA, Mow VC. Anisotropy, inhomogeneity, and tension–compression nonlinearity of human glenohumeral cartilage in finite deformation. *J Biomech*. 2005;38:799-809. doi:10.1016/j.jbiomech.2004.05.006
81. Ebrahimi M, Ojanen S, Mohammadi A, et al. Elastic, viscoelastic and fibril-reinforced Poroelastic material properties of healthy and osteoarthritic human tibial cartilage. *Ann Biomed Eng*. 2019;47:953-966. doi:10.1007/s10439-019-02213-4
82. Moo EK, Ebrahimi M, Sibole SC, Tanska P, Korhonen RK. The intrinsic quality of proteoglycans, but not collagen fibres, degrades in osteoarthritic cartilage. *Acta Biomater*. 2022;153:178-189. doi:10.1016/j.actbio.2022.09.002
83. Buckley MR, Bergou AJ, Fouchard J, Bonassar LJ, Cohen I. High-resolution spatial mapping of shear properties in cartilage. *J Biomech*. 2010;43:796-800. doi:10.1016/j.jbiomech.2009.10.012

84. Henak CR, Bartell LR, Cohen I, Bonassar LJ. Multiscale strain as a predictor of impact-induced fissuring in articular cartilage. *J Biomech Eng*. 2017;139:310041-310048. doi:10.1115/1.4034994
85. Couteau B, Labey L, Hobatho MC, et al. Validation of a three dimensional finite element model of a femur with a customized HIP implant. *Comput Methods Biomech Biomed Eng*. 1998;2:147-154. doi:10.1201/9781003078289-21
86. Taylor WR, Roland E, Ploeg H, et al. Determination of orthotropic bone elastic constants using FEA and modal analysis. *J Biomech*. 2002;35:767-773. doi:10.1016/S0021-9290(02)00022-2
87. Akizuki S, Mow VC, Müller F, Pita JC, Howell DS, Manicourt DH. Tensile properties of human knee joint cartilage: I. influence of ionic conditions, weight bearing, and fibrillation on the tensile modulus. *J Orthop Res*. 1986;4:379-392. doi:10.1002/jor.1100040401
88. DiSilvestro MR, Zhu Q, Wong M, Jurvelin JS, Suh J-KF. Biphasic poroviscoelastic simulation of the unconfined compression of articular cartilage: I—simultaneous prediction of reaction force and lateral displacement. *J Biomech Eng*. 2000;123:191-197. doi:10.1115/1.1351890
89. Brown CP, Nguyen TC, Moody HR, Crawford RW, Oloyede A. Assessment of common hyperelastic constitutive equations for describing normal and osteoarthritic articular cartilage. *Proc Inst Mech Eng H*. 2009;223:643-652. doi:10.1243/09544119JEIM546
90. Freutel M, Schmidt H, Dürselen L, Ignatius A, Galbusera F. Finite element modeling of soft tissues: material models, tissue interaction and challenges. *Clin Biomech*. 2014;29:363-372. doi:10.1016/j.clinbiomech.2014.01.006
91. Woo SL-Y, Akeson WH, Jemmott GF. Measurements of nonhomogeneous, directional mechanical properties of articular cartilage in tension. *J Biomech*. 1976;9:785-791. doi:10.1016/0021-9290(76)90186-X
92. Tomkoria S, Patel RV, Mao JJ. Heterogeneous nanomechanical properties of superficial and zonal regions of articular cartilage of the rabbit proximal radius condyle by atomic force microscopy. *Med Eng Phys*. 2004;26:815-822. doi:10.1016/j.medengphy.2004.07.006
93. Loparic M, Wirz D, Daniels AU, et al. Micro- and nanomechanical analysis of articular cartilage by indentation-type atomic force microscopy: validation with a gel-microfiber composite. *Biophys J*. 2010;98:2731-2740. doi:10.1016/j.bpj.2010.02.013
94. Darling EM, Topel M, Zauscher S, Vail TP, Guilak F. Viscoelastic properties of human mesenchymally-derived stem cells and primary osteoblasts, chondrocytes, and adipocytes. *J Biomech*. 2008;41:454-464. doi:10.1016/j.jbiomech.2007.06.019
95. Darling EM, Wilusz RE, Bolognesi MP, Zauscher S, Guilak F. Spatial mapping of the biomechanical properties of the pericellular matrix of articular cartilage measured in situ via atomic force microscopy. *Biophys J*. 2010;98:2848-2856. doi:10.1016/j.bpj.2010.03.037
96. Trickey WR, Lee GM, Guilak F. Viscoelastic properties of chondrocytes from normal and osteoarthritic human cartilage. *J Orthop Res*. 2000;18:891-898. doi:10.1002/jor.1100180607
97. Kääb MJ, Gwynn IA, Nötzli HP. Collagen fibre arrangement in the tibial plateau articular cartilage of man and other mammalian species. *J Anat*. 1998;193(Pt 1):23-34.
98. Raub CB, Unruh J, Suresh V, et al. Image correlation spectroscopy of multiphoton images correlates with collagen mechanical properties. *Biophys J*. 2008;94:2361-2373. doi:10.1529/biophysj.107.120006
99. Wilusz RE, DeFrate LE, Guilak F. Immunofluorescence-guided atomic force microscopy to measure the micromechanical properties of the pericellular matrix of porcine articular cartilage. *J R Soc Interface*. 2012b;9:2997-3007. doi:10.1098/rsif.2012.0314
100. Widuchowski W, Widuchowski J, Trzaska T. Articular cartilage defects: study of 25,124 knee arthroscopies. *Knee*. 2007;14:177-182. doi:10.1016/j.knee.2007.02.001
101. Danso EK, Honkanen JTJ, Saarakkala S, Korhonen RK. Comparison of nonlinear mechanical properties of bovine articular cartilage and meniscus. *J Biomech*. 2014;47:200-206. doi:10.1016/j.jbiomech.2013.09.015
102. Kerin AJ, Wisnom MR, Adams MA. The compressive strength of articular cartilage. *Proc Inst Mech Eng H*. 1998;212:273-280. doi:10.1243/0954411981534051
103. Chawla D, Eriten M, Henak CR. Effect of osmolarity and displacement rate on cartilage microfracture clusters failure into two regimes. *J Mech Behav Biomed Mater*. 2022;136:105467. doi:10.1016/j.jmbbm.2022.105467
104. Moo EK, Tanska P, Federico S, Al-Saffar Y, Herzog W, Korhonen RK. Collagen fibres determine the crack morphology in articular cartilage. *Acta Biomater*. 2021;126:301-314. doi:10.1016/j.actbio.2021.03.031
105. Orozco GA, Tanska P, Gustafsson A, Korhonen RK, Isaksson H. Crack propagation in articular cartilage under cyclic loading using cohesive finite element modeling. *J Mech Behav Biomed Mater*. 2022;131:105227. doi:10.1016/j.jmbbm.2022.105227
106. Si Y, Tan Y, Gao L, et al. Mechanical properties of cracked articular cartilage under uniaxial creep and cyclic tensile loading. *J Biomech*. 2022;134:110988. doi:10.1016/j.jbiomech.2022.110988
107. Zhou XQ, Yu DY, Shao XY, Zhang SQ, Wang S. Research and applications of viscoelastic vibration damping materials: a review. *Compos Struct*. 2016;136:460-480. doi:10.1016/j.compstruct.2015.10.014
108. Leipzig ND, Athanasiou KAKA. Unconfined creep compression of chondrocytes. *J Biomech*. 2005;38:77-85. doi:10.1016/j.jbiomech.2004.03.013
109. Chen C, Tambe DT, Deng L, Yang L. Biomechanical properties and mechanobiology of the articular chondrocyte. *Am J Physiol-Cell Physiol*. 2013;305:C1202-C1208. doi:10.1152/ajpcell.00242.2013
110. Mountcastle SE, Allen P, Mellors BOL, et al. Dynamic viscoelastic characterisation of human osteochondral tissue: understanding the effect of the cartilage-bone interface. *BMC Musculoskelet Disord*. 2019;20:575. doi:10.1186/s12891-019-2959-4
111. Temple DK, Cederlund AA, Lawless BM, Aspden RM, Espino DM. Viscoelastic properties of human and bovine articular cartilage: a comparison of frequency-dependent trends. *BMC Musculoskelet Disord*. 2016;17:419. doi:10.1186/s12891-016-1279-1
112. Miller GJ, Morgan EF. Use of microindentation to characterize the mechanical properties of articular cartilage: comparison of biphasic material properties across length scales. *Osteoarthr Cartil*. 2010;18:1051-1057. doi:10.1016/j.joca.2010.04.007
113. Maroudas A. Physicochemical properties of cartilage in the light of ion exchange theory. *Biophys J*. 1968;8:575-595.
114. Poole CA, Flint MH, Beaumont BW. Chondrons in cartilage: ultrastructural analysis of the pericellular microenvironment in adult human articular cartilages. *J Orthop Res*. 1987;5:509-522. doi:10.1002/jor.1100050406
115. García JJ, Cortés DH. A nonlinear biphasic viscohyperelastic model for articular cartilage. *J Biomech*. 2006;39:2991-2998. doi:10.1016/j.jbiomech.2005.10.017
116. Han L, Frank EH, Greene JJ, et al. Time-dependent nanomechanics of cartilage. *Biophys J*. 2011;100:1846-1854. doi:10.1016/j.bpj.2011.02.031
117. Wahlquist JA, DelRio FW, Randolph MA, et al. Indentation mapping revealed poroelastic, but not viscoelastic, properties spanning native zonal articular cartilage. *Acta Biomater*. 2017;64:41-49. doi:10.1016/j.actbio.2017.10.003
118. Fortin M, Soulhat J, Shirazi-Adl A, Hunziker EB, Buschmann MD. Unconfined compression of articular cartilage: nonlinear behavior and comparison with a fibril-reinforced biphasic model. *J Biomech Eng*. 1999;122:189-195. doi:10.1115/1.429641
119. Julkunen P, Korhonen RK, Herzog W, Jurvelin JS. Uncertainties in indentation testing of articular cartilage: a fibril-reinforced poroviscoelastic study. *Med Eng Phys*. 2008;30:506-515. doi:10.1016/j.medengphy.2007.05.012

120. Korhonen RK, Laasanen MS, Töyräs J, Lappalainen R, Helminen HJ, Jurvelin JS. Fibril reinforced poroelastic model predicts specifically mechanical behavior of normal, proteoglycan depleted and collagen degraded articular cartilage. *J Biomech*. 2003;36:1373-1379. doi:10.1016/S0021-9290(03)00069-1
121. Ateshian GA, Chahine NO, Basalo IM, Hung CT. The correspondence between equilibrium biphasic and triphasic material properties in mixture models of articular cartilage. *J Biomech*. 2004;37:391-400. doi:10.1016/S0021-9290(03)00252-5
122. Wilson W, van Donkelaar CC, van Rietbergen B, Huiskes R. A fibril-reinforced poroviscoelastic swelling model for articular cartilage. *J Biomech*. 2005a;38:1195-1204. doi:10.1016/j.jbiomech.2004.07.003
123. Ateshian GA, Maas S, Weiss JA. Multiphasic finite element framework for modeling hydrated mixtures with multiple neutral and charged solutes. *J Biomech Eng*. 2013;135(11):1-11. doi:10.1115/1.4024823
124. Räsänen LP, Tanska P, Mononen ME, et al. Spatial variation of fixed charge density in knee joint cartilage from sodium MRI - implication on knee joint mechanics under static loading. *J Biomech*. 2016;49:3387-3396. doi:10.1016/j.jbiomech.2016.09.011
125. Likhitpanichkul M, Guo XE, Mow V. The effect of matrix tension-compression nonlinearity and fixed negative charges on chondrocyte responses in cartilage. *Mol Cell Biomech MCB*. 2005;2:191-204. doi:10.3970/MCB.2005.002.191
126. Klika V, Gaffney EA, Chen Y-C, Brown CP. An overview of multiphase cartilage mechanical modelling and its role in understanding function and pathology. *J Mech Behav Biomed Mater*. 2016;62:139-157. doi:10.1016/j.jmbbm.2016.04.032
127. Ebrahimi M, Finnilä MAJ, Turkiewicz A, et al. Elastic, dynamic viscoelastic and model-derived fibril-reinforced Poroelastic mechanical properties of Normal and osteoarthritic human femoral condyle cartilage. *Ann Biomed Eng*. 2021;49:2622-2634. doi:10.1007/s10439-021-02838-4
128. Seifzadeh A, Wang J, Oguamanam DCD, Papini M. A nonlinear biphasic fiber-reinforced Porohyperviscoelastic model of articular cartilage incorporating fiber reorientation and dispersion. *J Biomech Eng*. 2011;133:81004-81008. doi:10.1115/1.4004832
129. Roberts JJ, Earnshaw A, Ferguson VL, Bryant SJ. Comparative study of the viscoelastic mechanical behavior of agarose and poly(ethylene glycol) hydrogels. *J Biomed Mater Res B: Appl Biomater*. 2011;99B:158-169. doi:10.1002/jbm.b.31883
130. Levett PA, Hutmacher DW, Malda J, Klein TJ. Hyaluronic acid enhances the mechanical properties of tissue-engineered cartilage constructs. *PLoS One*. 2014;9:1-24. doi:10.1371/journal.pone.0113216
131. Cigan AD, Roach BL, Nims RJ, et al. High seeding density of human chondrocytes in agarose produces tissue-engineered cartilage approaching native mechanical and biochemical properties. *J Biomech*. 2016;49:1909-1917. doi:10.1016/j.jbiomech.2016.04.039
132. Nasiri B, Mashayekhan S. Fabrication of porous scaffolds with decellularized cartilage matrix for tissue engineering application. *Biologicals*. 2017;48:39-46. doi:10.1016/j.biologicals.2017.05.008
133. Kim M, Erickson IE, Huang AH, Garrity ST, Mauck RL, Steinberg DR. Donor variation and optimization of human mesenchymal stem cell Chondrogenesis in hyaluronic acid. *Tissue Eng Part A*. 2018;24:1693-1703. doi:10.1089/ten.tea.2017.0520
134. Sivandzade F, Mashayekhan S. Design and fabrication of injectable microcarriers composed of acellular cartilage matrix and chitosan. *J Biomater Sci Polym Ed*. 2018;29:683-700. doi:10.1080/09205063.2018.1433422
135. Yang Z, Wu Y, Li C, et al. Improved mesenchymal stem cells attachment and In vitro cartilage tissue formation on chitosan-modified poly(l-Lactide-co-epsilon-Caprolactone) scaffold. *Tissue Eng Part A*. 2011;18:242-251. doi:10.1089/ten.tea.2011.0315
136. Rowland CR, Colucci LA, Guilak F. Fabrication of anatomically-shaped cartilage constructs using decellularized cartilage-derived matrix scaffolds. *Biomaterials*. 2016;91:57-72. doi:10.1016/j.biomaterials.2016.03.012
137. Zhou F, Zhang X, Cai D, et al. Silk fibroin-chondroitin sulfate scaffold with immuno-inhibition property for articular cartilage repair. *Acta Biomater*. 2017;63:64-75. doi:10.1016/j.actbio.2017.09.005
138. Gullotta F, Izzo D, Scalera F, et al. Biomechanical evaluation of hMSCs-based engineered cartilage for chondral tissue regeneration. *J Mech Behav Biomed Mater*. 2018;86:294-304. doi:10.1016/j.jmbbm.2018.06.040
139. Bhumiratana S, Eton RE, Oungoulian SR, Wan LQ, Ateshian GA, Vunjak-Novakovic G. Large, stratified, and mechanically functional human cartilage grown in vitro by mesenchymal condensation. *Proc Natl Acad Sci*. 2014;111:6940-6945. doi:10.1073/pnas.1324050111
140. Murphy MK, Huey DJ, Hu JC, Athanasiou KA. TGF-β1, GDF-5, and BMP-2 stimulation induces Chondrogenesis in expanded human articular chondrocytes and marrow-derived stromal cells. *Stem Cells*. 2015;33:762-773. doi:10.1002/stem.1890
141. Anderson DE, Markway BD, Weekes KJ, McCarthy HE, Johnstone B. Physioxia promotes the articular chondrocyte-like phenotype in human chondroprogenitor-derived self-organized tissue. *Tissue Eng Part A*. 2017;24:264-274. doi:10.1089/ten.tea.2016.0510
142. Cheng N-C, Estes BT, Awad HA, Guilak F. Chondrogenic differentiation of adipose-derived adult stem cells by a porous scaffold derived from native articular cartilage extracellular matrix. *Tissue Eng Part A*. 2008;15:231-241. doi:10.1089/ten.tea.2008.0253
143. Cheng N-C, Estes BT, Young T-H, Guilak F. Engineered cartilage using primary chondrocytes cultured in a porous cartilage-derived matrix. *Regen Med*. 2010;6:81-93. doi:10.2217/rme.10.87
144. Tanaka Y, Yamaoka H, Nishizawa S, et al. The optimization of porous polymeric scaffolds for chondrocyte/atelocollagen based tissue-engineered cartilage. *Biomaterials*. 2010;31:4506-4516. doi:10.1016/j.biomaterials.2010.02.028
145. Concaro S, Nicklasson E, Ellowsson L, Lindahl A, Brittberg M, Gatenholm P. Effect of cell seeding concentration on the quality of tissue engineered constructs loaded with adult human articular chondrocytes. *J Tissue Eng Regen Med*. 2008;2:14-21. doi:10.1002/term.60
146. Ando W, Tateishi K, Katakai D, et al. In vitro generation of a scaffold-free tissue-engineered construct (TEC) derived from human synovial mesenchymal stem cells: biological and mechanical properties and further chondrogenic potential. *Tissue Eng Part A*. 2008;14:2041-2049. doi:10.1089/ten.tea.2008.0015
147. Patel JM, Wise BC, Bonnevie ED, Mauck RL. A systematic review and guide to mechanical testing for articular cartilage tissue engineering. *Tissue Eng Part C: Methods*. 2019;25:593-608. doi:10.1089/ten.tec.2019.0116
148. Lammi MJ, Piltti J, Prittinen J, Qu C. Challenges in fabrication of tissue-engineered cartilage with correct cellular colonization and extracellular matrix assembly. *Int J Mol Sci*. 2018;19:2700. doi:10.3390/ijms19092700
149. Suo H, Zhang D, Yin J, Qian J, Wu ZL, Fu J. Interpenetrating polymer network hydrogels composed of chitosan and photocrosslinkable gelatin with enhanced mechanical properties for tissue engineering. *Mater Sci Eng C*. 2018;92:612-620. doi:10.1016/j.msec.2018.07.016
150. Wang C, Liu G, Zhang W, et al. Cartilage oligomeric matrix protein improves in vivo cartilage regeneration and compression modulus by enhancing matrix assembly and synthesis. *Colloids Surface B: Biointerfaces*. 2017;159:518-526. doi:10.1016/j.colsurfb.2017.08.008
151. Dusfour G, Maumus M, Cañadas P, et al. Mesenchymal stem cells-derived cartilage micropellets: a relevant in vitro model for biomechanical and mechanobiological studies of cartilage growth. *Mater Sci Eng C*. 2020;112:110808. doi:10.1016/j.msec.2020.110808

152. Henrionnet C, Wang Y, Roeder E, et al. Effect of dynamic loading on MSCs chondrogenic differentiation in 3-D alginate culture. *Biomed Mater Eng*. 2012;22:209-218. doi:10.3233/BME-2012-0710
153. Lu J, Fan Y, Gong X, et al. The lineage specification of mesenchymal stem cells is directed by the rate of fluid shear stress. *J Cell Physiol*. 2016;231:1752-1760. doi:10.1002/jcp.25278
154. Gadjanski I. Recent advances on gradient hydrogels in biomimetic cartilage tissue engineering. *F1000Research*. 2018;6:-1-9. doi:10.12688/f1000research.12391.2
155. Karimi T, Barati D, Karaman O, Moeinzadeh S, Jabbari E. A developmentally inspired combined mechanical and biochemical signaling approach on zonal lineage commitment of mesenchymal stem cells in articular cartilage regeneration. *Integr Biol*. 2015;7:112-127. doi:10.1039/c4ib00197d
156. Zhu D, Tong X, Trinh P, Yang F. Mimicking cartilage tissue zonal organization by engineering tissue-scale gradient hydrogels as 3D cell niche. *Tissue Eng Part A*. 2017;24:1-10. doi:10.1089/ten.tea.2016.0453
157. Zhu Y, Wu H, Sun S, Zhou T, Wu J, Wan Y. Designed composites for mimicking compressive mechanical properties of articular cartilage matrix. *J Mech Behav Biomed Mater*. 2014;36:32-46. doi:10.1016/j.jmbbm.2014.04.003
158. Chen H, Malheiro A d BFB, van Blitterswijk C, Mota C, Wieringa PA, Moroni L. Direct writing electrospinning of scaffolds with multidimensional fiber architecture for hierarchical tissue engineering. *ACS Appl Mater Interfaces*. 2017;9:38187-38200. doi:10.1021/acsami.7b07151
159. Kang H, Zeng Y, Varghese S. Functionally graded multilayer scaffolds for in vivo osteochondral tissue engineering. *Acta Biomater*. 2018;78:365-377. doi:10.1016/j.actbio.2018.07.039
160. Schipani R, Scheurer S, Florentin R, Critchley SE, Kelly DJ. Reinforcing interpenetrating network hydrogels with 3D printed polymer networks to engineer cartilage mimetic composites. *Biofabrication*. 2020;12:35011. doi:10.1088/1758-5090/ab8708
161. Engler AJ, Sweeney HL, Discher DE, Schwarzbauer JE. Extracellular matrix elasticity directs stem cell differentiation. *J Musculoskelet Neuronal Interact*. 2007;7:335.
162. Olivares-Navarrete R, Lee EM, Smith K, et al. Substrate stiffness controls osteoblastic and Chondrocytic differentiation of mesenchymal stem cells without exogenous stimuli. *PLoS One*. 2017;12:1-18. doi:10.1371/journal.pone.0170312
163. Steward AJ, Kelly DJ. Mechanical regulation of mesenchymal stem cell differentiation. *J Anat*. 2015;227:717-731. doi:10.1111/joa.12243
164. Klein TJ, Schumacher BL, Schmidt TA, et al. Tissue engineering of stratified articular cartilage from chondrocyte subpopulations. *Osteoarthr Cartil*. 2003;11:595-602. doi:10.1016/S1063-4584(03)00090-6
165. Cheung H-Y, Lau K-T, Lu T-P, Hui D. A critical review on polymer-based bio-engineered materials for scaffold development. *Compos Part B: Eng Bio-Eng Compos*. 2007;38:291-300. doi:10.1016/j.compositesb.2006.06.014
166. Huang J, Xiong J, Wang D, et al. 3D bioprinting of hydrogels for cartilage tissue engineering. *Gels*. 2021;7:144. doi:10.3390/gels7030144
167. Liu Y, Liu L, Wang Z, Zheng G, Chen Q, Luo E. Application of electrospinning strategy on cartilage tissue engineering. 2018;13:526-532. doi:10.2174/1574888X13666180628163515
168. Wang B, Chariyev-Prinz F, Burdis R, Eichholz K, Kelly DJ. Additive manufacturing of cartilage-mimetic scaffolds as off-the-shelf implants for joint regeneration. *Biofabrication*. 2022;14:024101. doi:10.1088/1758-5090/ac41a0
169. Abdel-Sayed P, Darwiche SE, Kettenberger U, Pioletti DP. The role of energy dissipation of polymeric scaffolds in the mechanobiological modulation of chondrogenic expression. *Biomaterials*. 2014;35:1890-1897. doi:10.1016/j.biomaterials.2013.11.048
170. Abdel-Sayed P, Moghadam MN, Salomir R, Tchernin D, Pioletti DP. Intrinsic viscoelasticity increases temperature in knee cartilage under physiological loading. *J Mech Behav Biomed Mater*. 2014;30:123-130. doi:10.1016/j.jmbbm.2013.10.025
171. Bakhshayesh ARD, Babaie S, Nasrabadi HT, Asadi N, Akbarzadeh A, Abedelahi A. An overview of various treatment strategies, especially tissue engineering for damaged articular cartilage. *Artif Cells Nanomed Biotechnol*. 2020;48:1089-1104. doi:10.1080/21691401.2020.1809439
172. Hassan CR, Qin Y-X, Komatsu DE, Uddin SMZ. Utilization of finite element analysis for articular cartilage tissue engineering. *Materials*. 2019;12:3331. doi:10.3390/ma12203331

How to cite this article: Petitjean N, Canadas P, Royer P, Noël D, Le Floc'h S. Cartilage biomechanics: From the basic facts to the challenges of tissue engineering. *J Biomed Mater Res*. 2022;1-23. doi:10.1002/jbm.a.37478